ChemInform Abstract: Radiolabeled Bioactive Benzoheterocycles for Imaging β-Amyloid Plaques in Alzheimer's Disease

ARTICLE *in* CHEMINFORM · OCTOBER 2014

Impact Factor: 0.74 · DOI: 10.1016/j.ejmech.2014.10.012 · Source: PubMed

2 AUTHORS:

Yanping Yang
Beijing Normal University
10 PUBLICATIONS **73** CITATIONS
SEE PROFILE

Meng-Chao Cui
Beijing Normal University
46 PUBLICATIONS **425** CITATIONS
SEE PROFILE

European Journal of Medicinal Chemistry 87 (2014) 703–721

Contents lists available at ScienceDirect

European Journal of Medicinal Chemistry

journal homepage: http://www.elsevier.com/locate/ejmech

Invited review

Radiolabeled bioactive benzoheterocycles for imaging β-amyloid plaques in Alzheimer's disease

Yanping Yang, Mengchao Cui*

Key Laboratory of Radiopharmaceuticals, Ministry of Education, College of Chemistry, Beijing Normal University, Beijing 100875, PR China

ARTICLE INFO

Article history:
Received 19 August 2014
Received in revised form
29 September 2014
Accepted 4 October 2014
Available online 7 October 2014

Keywords:
Alzheimer's disease
β-amyloid plaque
Radiolabeled
Benzoheterocycles
Imaging agents

ABSTRACT

Alzheimer's disease (AD) is a debilitating neurodegenerative dementia that involves substantial neuronal loss. Extracellular deposition of neurotoxic β-amyloid (Aβ) plaques in the brain has been recognized as the central histological characteristic of AD. In the past decade, precise detection of the Aβ plaques at preclinical AD with positron emission tomography (PET) or single photon emission computed tomography (SPECT) has achieved continued development. A big category of Aβ imaging agents was benzoheterocycles which derived from Thioflavin-T (ThT), a traditional amyloid binding dye. This review summarizes the past and current status of radioactive benzoheterocycles designed to selectively bind to Aβ plaques. Separate sections discuss the chemical synthesis, in vitro and in vivo investigations of radiolabeled benzothiazole, benzoxazole, benzofuran, benzothiophene, indole, imidazopyridine and quinoxaline analogs to act as PET/SPECT candidates for imaging Aβ plaques.

1. Introduction

Alzheimer's disease (AD) is a neurodegenerative disorder in which the death of brain neurons causes a set of symptoms including memory loss, cognitive decline, mood changes, and problems with communication, reasoning, and judgment. These symptoms will progress as the stages of Alzheimer's advance from preclinical (no impairment), mild cognitive impairment to dementia [1,2]. AD, as the most common form of dementia, accounts for 60%–80% of all cases. It potentially ranks as the third leading cause of death that as many as 500,000 Americans die of AD annually [3]. The world Alzheimer report 2013 reveals that 13% of people aged 60 or over need long-term care worldwide, as baby boomers age the total number will nearly treble from 101 to 277 million between 2010 and 2050 [4]. AD and related dementias place heavy burden on families and healthcare systems. It is estimated that one to four family members act as caregivers and the annual global cost of dementia care is currently over US$600 billion, namely around 1% of global GDP [4]. However, there is no known cure for AD since the death of brain cells cannot be halted or reversed. The best option is to identify AD at preclinical stage which can help initiate treatments as soon as possible, manage symptoms and improve quality of life.

Clinicians can now diagnose "probable" AD through patient history, a physical and neurological exam, blood and urine tests, brain scans with computed tomography (CT), magnetic resonance imaging (MRI) or electroencephalography (EEG). But these diagnostic tools are insufficient in sensitivity and accuracy, and AD can only be confirmed at postmortem or, in very rare cases, through a brain biopsy. Although the exact biological mechanism of AD pathology remains unclear, postmortem always show abnormal inclusions in the brain tissue: extracellular β-amyloid (Aβ) plaques and intracellular neurofibrillary tangles (NFTs) composed hyperphosphorylated tau proteins [2]. The amyloid cascade hypothesis suggests that the Aβ aggregates in the brain precede the onset of dementia and cognitive decline in AD patients [5]. Thus Aβ plaques in the brain are considered to be a good diagnostic and predictive biomarker of AD. Noninvasive nuclear imaging techniques including positron emission tomography (PET) and single-photon emission computed tomography (SPECT) are now moving into clinical practice and helping physicians to identify diseases in their earliest stages. The radionuclides most commonly used for PET imaging are ^{11}C ($t_{1/2}$ = 20.4 min) and ^{18}F ($t_{1/2}$ = 109.7 min), which can readily incorporated into bioactive molecules. Rapid decay of ^{11}C limits its use to facilities equipped with an onsite cyclotron, while ^{18}F with a longer half-life allows for an offsite cyclotron production and a longer in vivo investigation. For SPECT imaging, radionuclides ^{99m}Tc ($t_{1/2}$ = 6.01 h) and ^{123}I ($t_{1/2}$ = 13.2 h) are most widely used. In addition, ^{125}I ($t_{1/2}$ = 60.1 d) and ^{3}H ($t_{1/2}$ = 12.4 y) are usually employed for radioimmunoassay, in vitro binding assay,

* Corresponding author.
E-mail address: cmc@bnu.edu.cn (M. Cui).

http://dx.doi.org/10.1016/j.ejmech.2014.10.012
0223-5234/

autoradiography and some in vivo investigations. PET/SPECT can provide detailed pictures of activities and functions inside the body and enable physicians to measure the chemical and biological processes. Therefore, imaging Aβ plaques by PET/SPECT with radiolabeled molecules able to bind the Aβ fibrils could aid in achieving presymptomatic diagnosis of AD patients and accurately assessing the effectiveness of ongoing therapeutic strategies.

To accomplish this goal, development of Aβ-specific imaging agents has been intensively pursued. An ideal Aβ imaging candidate would combine a high binding affinity for Aβ plaques ($K_i \leq 20$ nM) with low nonspecific binding and excellent pharmacokinetics with a high initial brain uptake (>5 %ID/g at 2 min post-injection) and a rapid washout from normal brain regions ($brain_{2\ min}/brain_{60\ min}$ ratio > 3.5) [6,7]. Initial structural inspiration came from Congo red (CR) and Thioflavin-T (ThT), traditional amyloid binding dyes used in autopsy. Several recent review papers have generally summarized the biological properties of CR analogs, ThT analogs, stilbene analogs and the plant pigments based Aβ imaging probes [7–10]. Among the reported Aβ probes, a big group of ThT derived Aβ-specific ligands with conjugated benzoheterocyclic rings was one of the most studied Aβ imaging families (Fig. 1). These chemical scaffolds all held the relatively planar, hydrophobic aromatic properties of ThT, which allows for their insertion into the cross-β sheet structure of Aβ plaques. Zeng et al. have summarized the ^{18}F-labeled heterocycles for PET imaging of Aβ plaques, however the ^{11}C-, ^{123}I- and ^{99m}Tc-labeled heterocycles were not included in this review [11]. In addition, the scaffolds listed were incomplete without covering the benzothiophene, indole and quinoxaline cores. Thus, this review will focus on providing an overview of these radiolabeled bioactive benzoheterocyclics as Aβ imaging candidates, with a particular elaboration of the cyclization strategies for the benzoheterocyclic rings, as well as characteristics, binding abilities, in vivo pharmacokinetics of the Aβ-specific benzoheterocyclics. According to the type of benzoheterocyclic scaffolds, we make the discussion in divided sections including radiolabeled benzothiazole, benzoxazole, benzofuran, benzothiophene, indole, imidazopyridine and quinoxaline analogs.

2. Binding mechanism of Thioflavin-T to amyloid fibrils

Superior to Congo red and methyl violet, the benzothiazole dye ThT has been the most commonly used histological agent for detecting amyloid deposits over a long time [12]. Substantial researches have been conducted to elucidate the molecular interaction of ThT with amyloid fibrils. In solution, the free ThT could rotate around the middle carbon–carbon bond shared by the benzothiazole and aminobenzoyl rings, leading to a twisted, chiral conformation (Fig. 2A) [13]. The aromatic side-chain ladders on the cross-β sheet surfaces of amyloid fibrils gave rise to binding sites for ThT (Fig. 2B) [14]. Computational simulations demonstrated that ThT inserted into the binding channels formed by aromatic residues on the flat β-sheet surface, orientating along the long axis of the fibrils (Fig. 2D and E) [15]. Upon binding to amyloid fibrils, the ThT was sterically locked by the binding channels. This rotational immobilization preserved the excited state generated by photon excitation, thus resulting in a dramatic increase of ThT fluorescence (Fig. 2C). In addition, ThT underwent a significant shift of the excitation maximum from 385 nm to 450 nm and the emission maximum from 445 nm to 482 nm [13].

3. Benzothiazole derivatives

Using benzothiazole scaffold as a building moiety has developed a wide array of Aβ imaging agents over the last few years. Of them, benzothiazole aniline (BTA) derivatives are one of the most prolific and promising family of imaging agents targeting to Aβ plaques. Three main routes have been adopted for the preparation of the BTA scaffold. The thoroughly applied one is a linear approach (Scheme 1, Approach A), which converts the benzoyl amides to corresponding thioamides by Lawesson's reagent and followed by classical cyclization using an oxidant (for instance $K_3Fe(CN)_6$) under Jacobson's conditions [16–18]. Though this cyclization is highly substituent dependent, it remains to be versatile for the high availability of the diverse substituted anilines. When a specific substituted 2-aminobenzenethiol is readily available, another process (Scheme 1, Approach B) seems to be more competitive and straightforward, particularly for the preparation of secondary or tertiary amine substituted BTAs. A one-pot condensation of a 2-aminothiophenol and a benzaldehyde, benzoic acid or benzoyl chloride derivative could conveniently form the BTA backbone [16,19]. These reactions are performed under harsh conditions with a Lewis acid (for instance polyphosphoric acid) and sometimes at high temperatures. Another efficient method also illustrates this approach. The one-pot reaction of an anionically activated aromatic/heteroaromatic trifluoromethyl group with the NH_2 and SH nucleophiles of 2-aminobenzenethiol under a mild aqueous

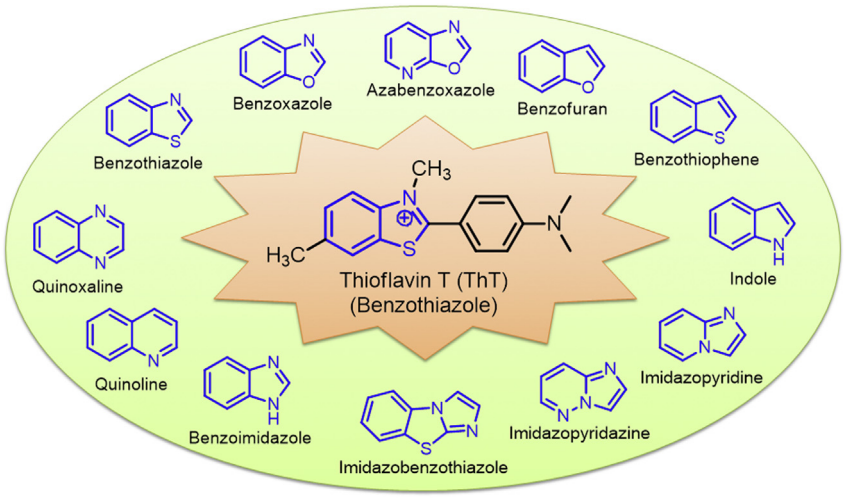

Fig. 1. Benzoheterocyclic scaffolds derived from Thioflavin-T.

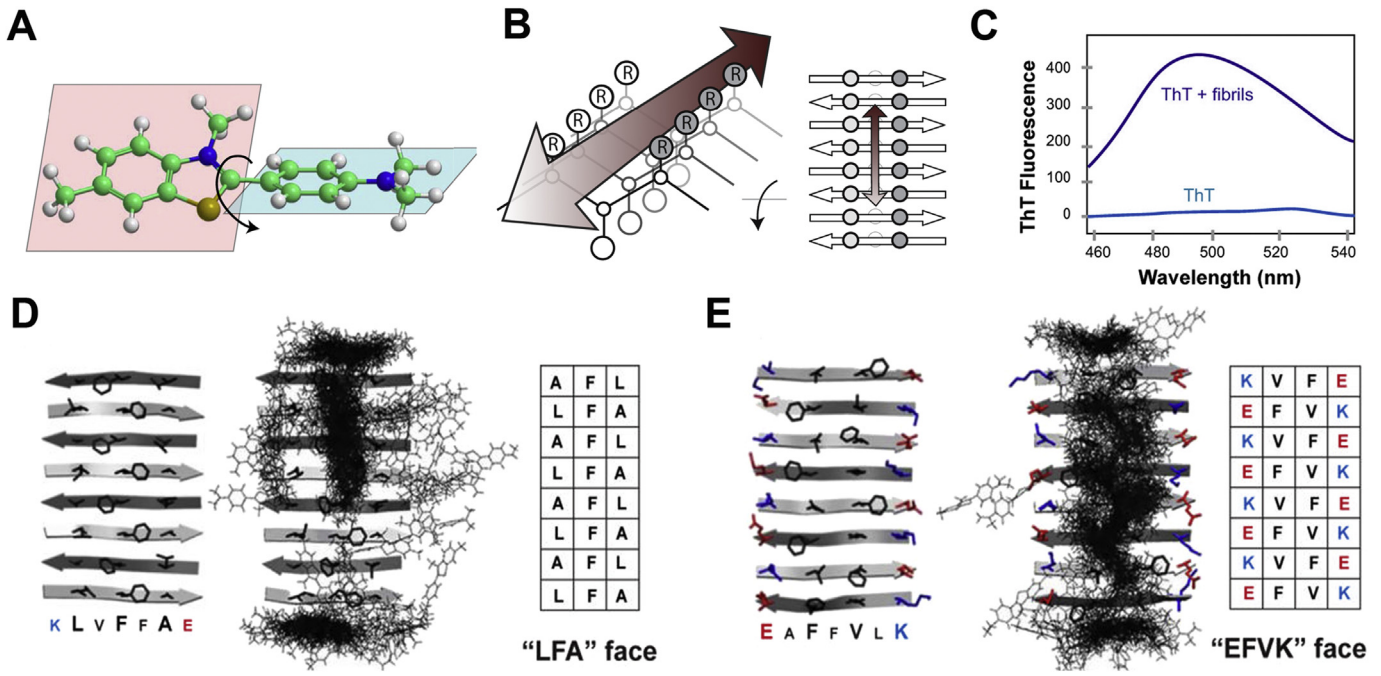

Fig. 2. Binding mechanism of ThT to amyloid fibrils. (A) Twisted and chiral conformation of ThT generated by rotation. (B) ThT was proposed to insert into the side-chain cavities on the flat surface of fibrils running along the long axis. (C) The enhancement of ThT fluorescence after binding to amyloid fibrils. (D–E) Distribution of the bound ThT around the KLVFFAE protofibril probed using molecular dynamics simulations. Adapted from Ref. [13].

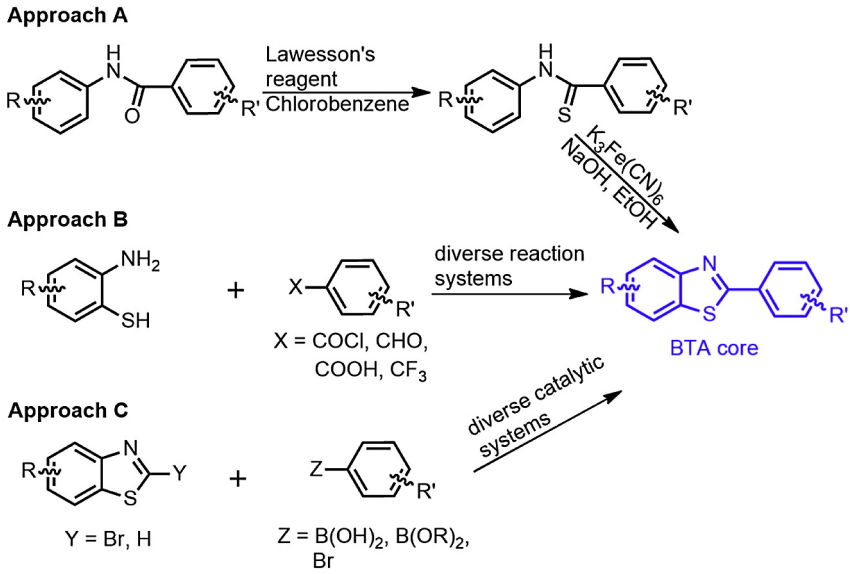

Scheme 1. Three general synthetic approaches leading to the benzothiazole aniline (BTA) core.

condition (for instance 1 M sodium hydroxide) provides an alternative access to the 2-arylbenzothiazoles [20]. This synthetic strategy for C–C linked aryl-heterocycles or heteroaryl-heterocycles is high functional group tolerable and potentially useful in parallel synthesis. Additional two types of direct arylation have been described for preparing of the BTA backbone: C–H activation and Suzuki–Miyaura coupling (Scheme 1, Approach C). A new direct arylation of benzothiazole through metal-catalyzed (palladium and copper) C–H bond activation with an aryl halide or boronic acid offers a simple pathway to access BTA core [21,22]. Suzuki–Miyaura reaction also provides an efficient access to the BTA backbone through Pd (II) or Cu (I) catalyzed cross-coupling between 2-bromobenzothiazoles and aryl-boron species [23,24]. As a wide array of the starting reagents is commercially available, this cross-coupling strategy might be favored, especially for structure–activity relationship (SAR) studies.

Removal of the methyl substituent on N^3 of ThT offered neutral and more lipophilic molecules, which are expected to exhibit high blood–brain barrier (BBB) permeability. Klunk et al. reported the earliest radiolabeled BTA derivatives, [^{11}C]6-Me-BTA-1 (Table 1, **1**), with higher binding affinity towards Aβ_{40} aggregates ($K_i = 20.2$ nM) than ThT ($K_i = 890$ nM) [25]. Fluorescent staining on postmortem AD brain sections revealed that 6-Me-BTA-1 stained both plaques and tangles, as did ThT. And 6-Me-BTA-1 showed more intense

Table 1
Binding affinities and brain pharmacokinetics of ^{11}C- and ^{125}I-labeled benzothiazole aniline derivatives (BTAs).

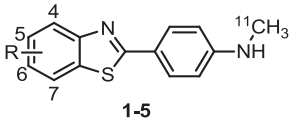

1-5

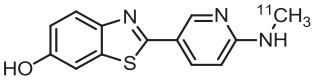

6 = [^{11}C]AZD2184

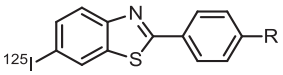

7-8

Compound	R	$A\beta_{40}$ K_i (nM)	Brain uptake (%ID/g)		Ref.
			2 min	60 min	
ThT	–	890	–	–	[25]
1 (6-Me-BTA-1)	6-Me	20.2	7.61	1.29	[25]
2 (PIB)	6-OH	4.3	0.21[b]	0.018[b,c]	[16]
3	4-OH	18.8[a]	3.8	0.30	[29]
4	5-OH	11.5[a]	4.3	0.09	[29]
5	7-OH	11.2[a]	2.6	0.16	[29]
6 (AZD2184)	–	8.4[d]	1.0[e]	–	[31]
7 (TZDM)	NMe_2	0.9	0.6[f]	1.57[f]	[32]
8 (TZPI)	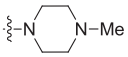	5.4	1.50[f]	1.89[f]	[32]

[a] Expressed as binding to amyloid plaques in human AD brain homogenates.
[b] Expressed as (%ID-kg)/g in mice.
[c] Expressed as 30 min post-injection.
[d] Expressed as K_d for $A\beta_{40}$ aggregates.
[e] Expressed as %ID/organ in rats.
[f] Expressed as %ID/organ in mice.

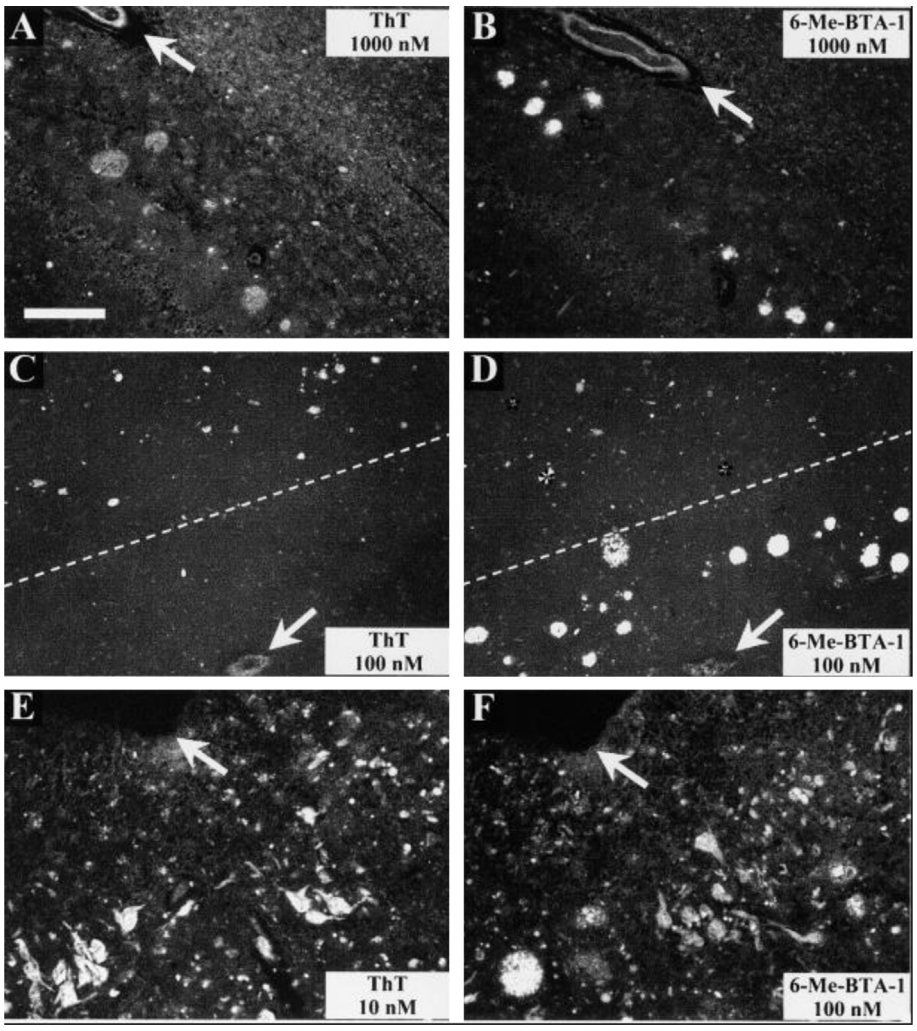

Fig. 3. Fluorescent staining of ThT and 6-Me-BTA-1 on brain sections of a single AD case. Arrows point out vessels (A–D) or cortical surface landmarks (E & F). Adapted from Ref. [25].

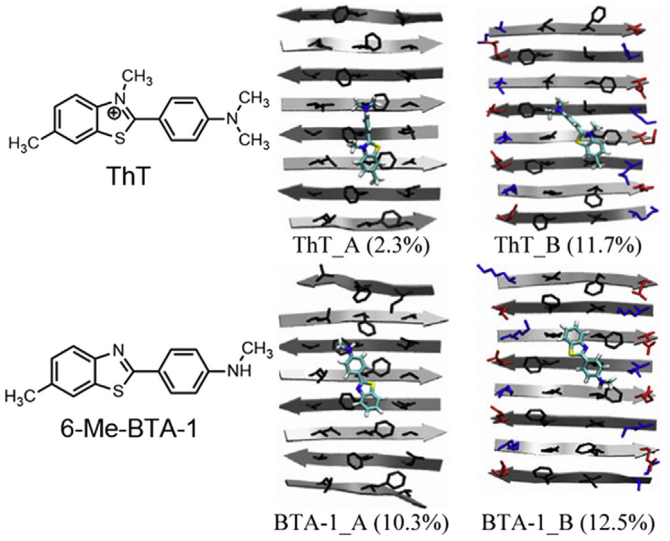

Fig. 4. Two main binding modes of ThT and 6-Me-BTA-1 to the amyloid fibrils. Atoms C, N, S and H of the compounds were colored by cyan, blue, yellow and white, respectively. The positively charged, negatively charged and hydrophobic side-chains of the fibrils were colored in blue, red and black, respectively. Adapted from Ref. [15]. (For interpretation of the references to colour in this figure legend, the reader is referred to the web version of this article.)

labeling for plaques than ThT under these conditions, but less intense for NFTs (Fig. 3) [25]. Molecular dynamics simulations were performed to identify the binding models of ThT and its neutral analog 6-Me-BTA-1 on Aβ fibrils [15]. For both ThT and 6-Me-BTA-1, the dominant binding sites were the central pockets on the β-sheet surface along the β-sheet extension orientation (Fig. 4). Meanwhile, the positive charged ThT did not bind to the negatively charged Glu22, indicating that charge–charge interaction may not be critical for recognizing the amyloid fibrils. Thus removing the positive charge of ThT would not alter the binding models [15]. Furthermore, ThT showed rapid binding to and dissociation from the grooves on the fibril surface, which was in accordance with its lower binding affinity [13]. [^{11}C]6-Me-BTA-1 displayed high initial brain uptake (7.61 %ID/g at 2 min) and good washout from normal brain tissue (1.29 %ID/g at 60 min) [25]. Additional modifications of this backbone resulted in a series of ^{11}C-labeled BTA analogs, of which [N-methyl-^{11}C]6-OH-BTA-1 (Table 1, **2**) with 6-OH group, well-known as [^{11}C]PIB, displayed good binding affinity for Aβ_{40} aggregates (K_i = 4.3 nM), moderate brain uptake (0.21 (%ID-kg)/g at 2 min) and excellent clearance (0.018 (%ID-kg)/g at 30 min) [16,17]. Approach A was applied to synthesize the PIB precursor (4-(6-(methoxymethoxy)benzo[d]thiazol-2-yl)aniline or 2-(4-aminophenyl)benzo[d]thiazol-6-ol), while the standard PIB compound was obtained through approach B [16]. After the toxicologic and animal physiological studies, first human study with [^{11}C]PIB was identified in 2002, and then thousands of [^{11}C]PIB PET scans have been conducted in AD patients all around the world [26–28]. [^{11}C]PIB showed specific binding to the amyloid-laden parietal and frontal cortices of AD brains, but little retention in the amyloid-free healthy control brains, indicating low levels of non-specific binding. Besides, [^{11}C]PIB possessed rapid entry and clearance in all cortical and subcortical white matter areas of healthy control subjects. In cortical areas, the marked difference between [^{11}C]PIB images from AD patients and healthy subjects were apparent, suggesting that PET imaging with [^{11}C]PIB could provide quantitative information on Aβ plaques and aid in early diagnose of AD patients. To investigate the structure activity relationship of the position of the hydroxyl group, three analogs of PIB with 4-hydroxy, 5-hydroxy and 7-hydroxy substituents (Table 1, **3**–**5**) were synthesized, ^{11}C-labeled and biological evaluated [29]. The BTA core was obtained through methods similar to PIB (Scheme 1, approach A for the primary amine precursors and approach B for the secondary amine standard compounds). Molecules **3**–**5** exhibited good binding abilities for Aβ plaques in human AD brain homogenates (K_i = 11–19 nM), but they are slightly inferior to PIB (K_i = 2.8 nM, tested with the identical assay). The 5-hydroxy derivative [^{11}C]**4** displayed best brain pharmacokinetic profile with a suitable initial uptake (4.3 %ID/g) and a rapid washout ($brain_{2\ min}/brain_{60\ min}$ ratio = 47.8), which was 8 times faster than that of [^{11}C]PIB. To reduce the lipophilicity and improve signal-to-background ratio, [^{11}C]AZD2184 (Table 1, **6**) was developed by replacing the phenyl moiety with a pyridyl moiety [24,30,31]. BTA core of AZD2184 was

Table 2
Binding affinities and brain pharmacokinetics of ^{18}F-fluoroalkylated and fluoro-pegylated benzothiazole aniline derivatives (BTAs).

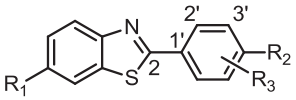

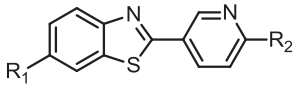

Compound	R_1	R_2	R_3	Aβ_{40} K_i (nM)	Brain uptake (%ID/g)		Ref.
					2 min	60 min	
9 (FBTA)	OH	$NHEt^{18}F$	H	–	0.1[b]	0.029[b,c]	[33]
10 (O-FEt-PIB)	$OEt^{18}F$	NHMe	H	0.17[a]	0.64[b]	0.09[b]	[34]
11 (3′-FEtO-BTA-0)	H	NH_2	3′-$OEt^{18}F$	≥600	7.0	1.7	[36]
12	$OPr^{18}F$	NH_2	H	14.5[a]	4.5	1.2	[37]
13	H	NH2	2′-$OPr^{18}F$	≥4000[a]	3.0	0.7	[37]
14	$(OEt)_2^{18}F$	NHMe	H	2.2[a]	10.27	3.94	[38]
15	$(OEt)_3^{18}F$	NHMe	H	3.8[a]	5.53	2.18	[38]
16	$(OEt)_6^{18}F$	NHMe	H	4.7[a]	2.57	1.80	[38]
17	$(OEt)_3^{18}F$	NHMe	–	9.3[d]	2.23	1.26	[39]
18	$(OEt)_3^{18}F$	NMe_2	–	5.8[d]	3.26	1.84	[39]
19	$OEt^{18}F$	NHMe	–	10.1[d]	7.87	2.83	[39]

[a] Expressed as binding to amyloid plaques in human AD brain homogenates.
[b] Expressed as (%ID-kg)/g in mice.
[c] Expressed as 30 min post-injection.
[d] Expressed as K_i for Aβ_{42} aggregates.

Table 3
Binding affinities and brain pharmacokinetics of benzothiazole aniline derivatives with ^{18}F-atom directly attached to the aromatic ring.

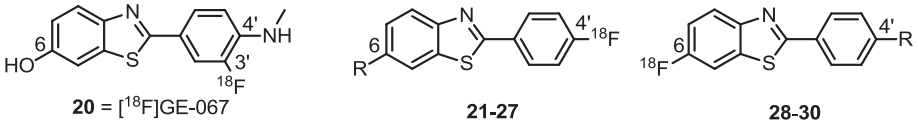

Compound	R	$A\beta_{42}$ K_i (nM)	Brain uptake (%ID/g)		Ref.
			2 min	60 min	
20 (GE-067)	–	5.9[a]	3.67[b]	0.20	[40,42]
21	H	9.0[c]	3.20	0.21	[46]
22	6-OMe	2.2[c]	5.10	0.43	[47]
23	6-OH	22.5[c]	4.70	0.57	[47]
24 (KS-28)	6-Me	5.7[c]	5.33	0.27	[47]
25	6-NH_2	10.0[c]	13.97	0.97	[48]
26	6-NHMe	4.1[c]	12.13	1.39	[48]
27	6-NMe_2	3.8[c]	8.84	1.94	[48]
28	NH_2	26.2	5.86	0.73	[49]
29	NHMe	5.5	6.62	0.73	[49]
30	NMe_2	5.9	4.39	1.61	[49]

[a] Expressed as K_i for $A\beta_{40}$ aggregates.
[b] Expressed as 5 min post-injection in rats.
[c] Expressed as binding to amyloid plaques in human AD brain homogenates.

obtained through a palladium catalyzed Suzuki–Miyaura cross-coupling between substituted 2-bromobenzothiazole and starting pyridyl boronic acid or ester (Scheme 1, Approach C). Comparing with [^{11}C]PIB, [^{11}C]AZD2184 labeled $A\beta$ plaques with decreased non-specific background binding levels and provided higher contrast images by PET measurements on AD patients and control subjects. Besides carbon-11, iodine-123/125 has been used for radiolabeling of SPECT imaging agents, resulting in two

Table 4
Brain pharmacokinetics of ^{99m}Tc-labeled 2-phenylbenzothiazole derivatives.

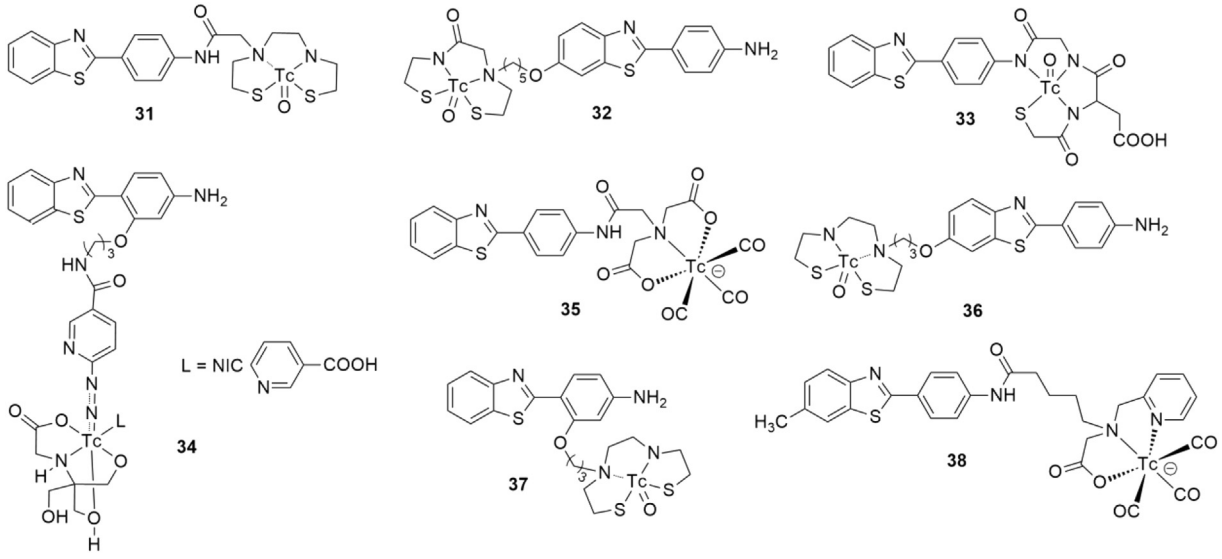

Compound	Brain uptake (%ID/g)		Ref.
	2 min	60 min	
31	0.09[a]	0.03[a]	[50]
32	1.34	0.65	[51]
33	0.28	0.20	[52]
34	0.38	0.17	[52]
35	0.07	0.03	[52]
36	0.5	0.3	[53]
37	0.2	0.2	[53]
38	0.69[b]	0.02	[54]

[a] Expressed as %ID/organ in mice.
[b] Expressed as brain uptake at 1 min post-injection.

radioiodinated BTAs, TZDM and TZPI (Table 1, **7** and **8**) [32]. Scheme 1, approach B was adopted to prepare the BTA core for these two compounds by condensation of 2-amino-5-bromobenzenethiol and corresponding benzaldehydes. Autoradiography of [^{125}I]TZDM and [^{125}I]TZPI showed distinctive labeling of the Aβ plaques on sections from a postmortem Down's syndrome brain. However, both of them displayed long retention in the normal brain with high radioactive levels of 1.57 and 1.89 %ID/organ at 60 min post-injection, respectively. This disfavored brain pharmacokinetic may be attributed to the relative high lipophilicity caused by incorporation of iodine atom.

However, the short half-life of ^{11}C ($t_{1/2}$ = 20.4 min) limits its use to PET centers with an onsite cyclotron. The development of ^{18}F ($t_{1/2}$ = 109.7 min) labeled BTA derivatives would extend the availability of the radioligands. Besides, the longer half-life of ^{18}F may reduce the non-specific background binding through prolongation of the washout time, providing improved signal-to-noise ratio. Based on the structure of PIB, a series of fluorinated BTA compounds have been reported. The ^{18}F labeling was achieved by attaching a fluoroalkyl chain to the backbone via a nucleophilic fluorination with good leaving groups such as tosylate or mesylate precursors (Table 2, **9**–**13**). Replacing the [^{11}C]methylamino group of [^{11}C]PIB with a [^{18}F]fluoroethylamino group resulted in a ^{18}F-labeled BTA ligand [^{18}F]FBTA (Table 2, **9**) [33]. In ligand [^{18}F]O-FEt-PIB (Table 2, **10**), the [^{18}F]fluoroethoxy group was moved to the 6-position, and this ligand possessed high binding affinity for amyloid plaques in human AD brain homogenates (K_i = 0.17 nM) [34,35]. Attaching the fluoroethoxy substituent to the 2-phenyl ring generated another fluorinated BTA derivatives, [^{18}F]3′-FEtO-BTA-0 (Table 2, **11**) [36]. Two fluoropropoxy substituted phenylbenzothiazoles (Table 2, **12**, **13**) were also synthesized, radiolabeled and biologically evaluated [37]. Surprisingly, position isomers **11** ($K_i \geq$ 600 nM) and **13** ($K_i \geq$ 4000 nM) with fluoroalkyl substituents on 3′- and 2′-position displayed much lower binding abilities than corresponding 6-position substituted ligands **10** (K_i = 1.7 nM) and **12** (K_i = 14.5 nM). This low binding potential may be ascribed to the torsion of the bond between carbon-2 and carbon-1′ caused by the steric substitution on the 2′- and 3′-position of the 2-phenyl ring, leading to a non-planar conformation which is unable to bind to amyloid [37]. Besides, the introducing of a fluoroalkyl chain would increase the lipophilicity, resulting in higher non-specific binding and slightly worse brain pharmacokinetic. In an attempt to modulate the lipophilicity and modify the pharmacokinetic properties of ^{18}F-labeled BTA molecules, Kung et al. adopted a pegylation-fluorination strategy, leading to a series of fluoro-pegylated BTA derivatives (Table 2, **14**–**16**) with a short length of fluoropolyethylene glycol (FPEG) ($n \leq 8$) chain at 6-position of the core structure [38]. The three resulted FPEG-PIB conjugates retained appropriate lipophilicity (log P = 2.99–3.04) and high binding affinities (K_i = 2.2–4.7 nM) comparable to PIB. However, lengthening the PEG chain lead to a gradual decline in initial brain uptake (**14**: n = 2, 10.27 %ID/g; **15**: n = 3, 5.53 %ID/g; **16**: n = 6, 2.57%ID/g). Besides, they displayed much lower washout rates than the lead compound PIB ($brain_{2\ min}/brain_{60\ min}$ ratio < 3). To further decrease the lipophilicity, Cui et al. reported three fluoro-pegylated 2-pyridylbenzothiazole ligands with a bioisosteric 2-pyridyl moiety (Table 2, **17**–**19**) [39]. The BTA backbone was formed via a convenient one-pot reaction of anionically activated 5-(trifluoromethyl)pyridin-2-amine and 2-amino-5-methoxybenzenethiol under a mild aqueous condition (NaOH, 1 M) (Scheme 1, Approach B). Similarly, compounds **17**–**19** all possessed high affinity for Aβ fibrils but undesirable in vivo brain pharmacokinetics.

Table 5
Binding affinities and brain pharmacokinetics of benzothiazole derivatives **39**–**51**.

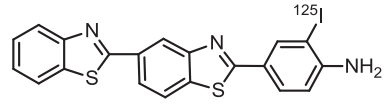

39

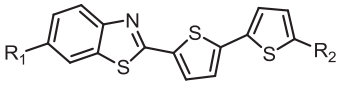

40-41

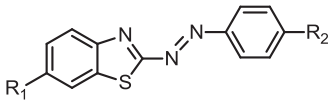

42-45

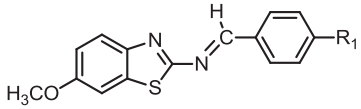

46-51

Compound	R_1	R_2	Aβ_{42} K_i (nM)	Brain uptake (%ID/g)		Ref.
				2 min	60 min	
39	–	–	21[a]	3.71	0.43	[55]
40	^{125}I	H	0.31	3.42	0.53	[56]
41	OMe	^{125}I	0.61	0.87	0.77	[56]
42	^{125}I	NH_2	6.40	0.96[b]	3.23[b]	[57]
43	^{125}I	NHMe	5.08	1.03[b]	3.13[b]	[57]
44	^{125}I	NMe_2	8.24	0.94[b]	2.89[b]	[57]
45 (FPPDB)	$(OEt)_3^{18}F$	NMe_2	20.0	4.28	2.53	[58]
46	NMe_2	–	4.38[a]	–	–	[59]
47	NO_2	–	514.65[a]	–	–	[59]
48	OMe	–	10.82[a]	–	–	[59]
49	Br	–	106.46[a]	–	–	[59]
50	I	–	102.74[a]	–	–	[59]
51	OH	–	34.72[a]	–	–	[59]

[a] Expressed as binding to amyloid plaques in human AD brain homogenates.
[b] Expressed as %ID/organ in normal mice.

Table 6
Binding affinities and brain pharmacokinetics of 2-arylbenzoxazole derivatives **52**–**63**.

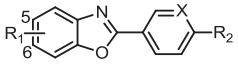

52-63

Compound	R_1	R_2	X	$A\beta_{42}$ K_i (nM)	Brain uptake (%ID/g)		Ref.
					2 min	60 min	
52 (IBOX)	6-^{125}I	NMe_2	CH	0.8[a]	1.43[b]	1.26[b]	[60]
53	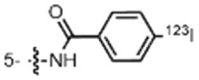	NMe_2	CH	9.3	–	–	[62]
54	6-OH	NHC^3H_3	N	182[c]	0.5[b]	–	[63]
55	6-OH	$NHEt^{18}F$	N	158[c]	0.3[b]	–	[64]
56	6-OMe	$NHEt^{18}F$	N	35[c]	0.4[b]	–	[64]
57	6-OH	$NHPr^{18}F$	N	395[c]	–	–	[64]
58	5-$(OEt)_3^{18}F$	NHMe	CH	9.3	8.12	3.04	[66]
59	5-$(OEt)_3^{18}F$	NMe_2	CH	3.9	5.29	2.12	[66]
60	5-$(OEt)_3^{18}F$	NHMe	N	76.9	4.05	1.78	[39]
61	5-$(OEt)_3^{18}F$	NMe_2	N	9.9	3.79	1.82	[39]
62	5-O$Et^{18}F$	NHMe	N	8.0	7.23	1.55	[39]
63	5-O$Et^{18}F$	NMe_2	N	2.7	7.27	1.47	[39]

[a] Expressed as K_i for $A\beta_{40}$ aggregates.
[b] Expressed as %ID/organ in normal mice.
[c] Expressed as IC_{50} for $A\beta_{40}$ aggregates.

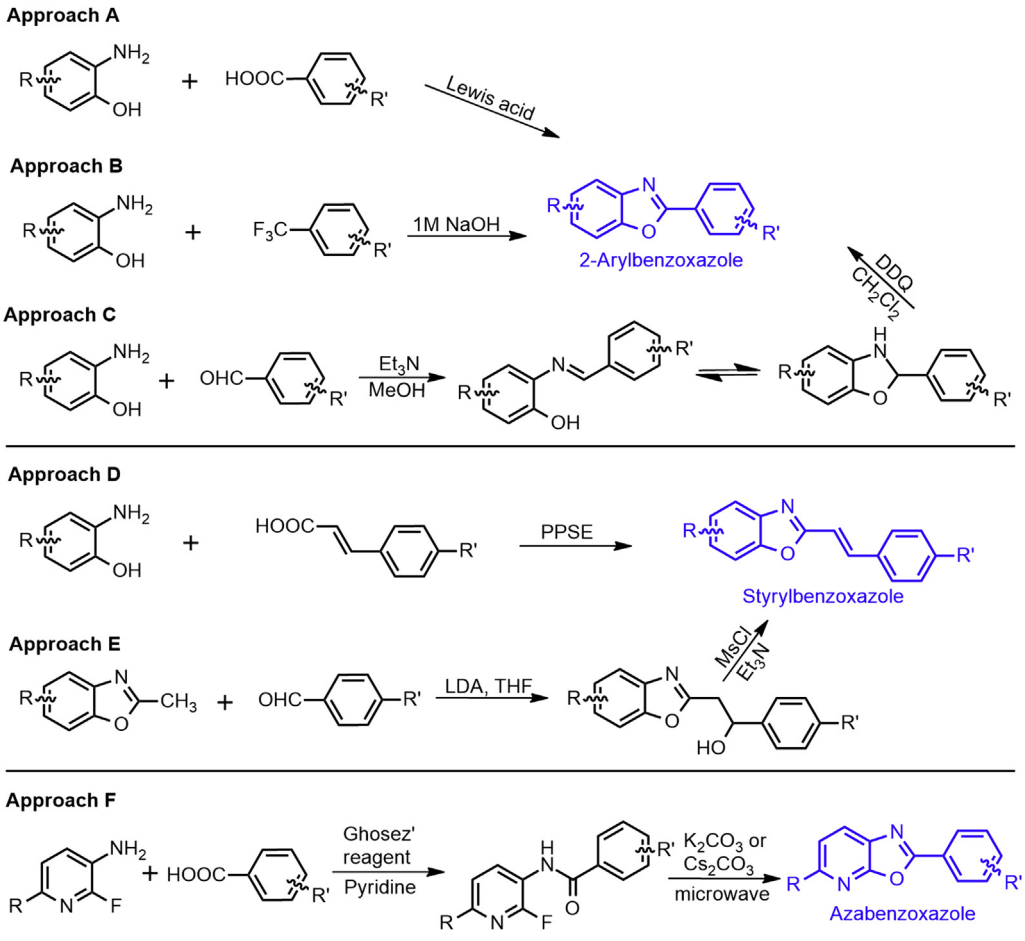

Scheme 2. General synthetic approaches to the benzoxazole core.

Table 7
Binding affinities and brain pharmacokinetics of styrylbenzoxazole and azabenzoxazole derivatives **64**–**71**.

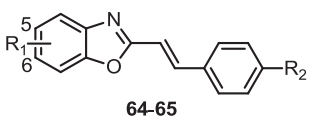

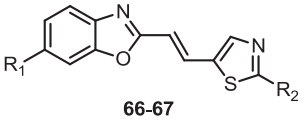

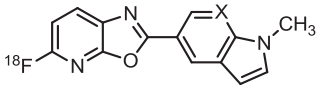

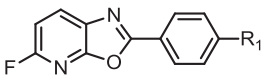

Compound	R_1	R_2	$A\beta_{42}$ K_i (nM)	Brain uptake (%ID/g)		Ref.
				2 min	60 min	
64 (BF-145)	5-F	$NH^{11}CH_3$	6.4	4.4	1.6[a]	[67]
65 (BF-168)	6-$OEt^{18}F$	NHMe	4.5	3.9	1.3	[68]
66 ([^{11}C]BF-227)	OEtF	$NMe^{11}CH_3$	4.3	7.9	0.64	[70]
66 ([^{18}F]BF-227)	$OEt^{18}F$	NMe_2	4.3	6.05	1.67	[72]
67 (FACT)	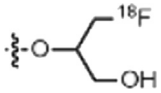	NMe_2	–	4.64	0.28	[72]
68 (MK-3328)	–	–	10.5[b]	–	–	[75]
69 (AD-269)	–	–	8.0[b]	–	–	[75]
70 (AD-278)	NMe_2	–	4.0[b]	–	–	[75]
71 (AD-265)	NHMe	–	17[b]	–	–	[75]

[a] Expressed as brain uptake at 30 min post-injection.
[b] Expressed as IC_{50} for human AD brain cortical homogenates.

Several ^{18}F-labeled BTAs with the ^{18}F-atom directly attached to the aromatic ring have been reported. The ^{18}F atom was introduced mainly through an aromatic nucleophilic substitution with the nitro precursors. [^{18}F]3′-F-PIB (also known as [^{18}F]GE-067, ^{18}F-flutemetamol, and Vizamyl™, Table 3, **20**), as a 3′-F analog of PIB, was the second imaging agent to be approved by U.S. Food and Drug Administration (U.S. FDA) for lighting up clusters of β-amyloid in the brain [40]. [^{18}F]GE-067 displayed similar binding affinities ($K_i = 5.9$ nM), brain pharmacokinetics in Sprague Dawley rats (3.67 %ID/g at 5 min and 0.20 %ID/g at 60 min post-injection), metabolism and dosimetry to the established [^{11}C]PIB and other ^{18}F-labeled radiopharmaceuticals, but somewhat higher non-specific retention in subcortical white matter was observed relative to [^{11}C]PIB [40–43]. Scans with [^{18}F]GE-067 can reliably identify and quantify cortical Aβ deposits by the use of relative standard uptake value ratios, using the cerebellar cortex as a reference region. Rapid uptake into the brain and high sensitive and specific binding to Aβ deposits were demonstrated in clinical trials in discriminating between AD patients and healthy controls, promoting its approval to assist in accurate detection of β-amyloid in living patients [44,45]. To further take the advantage of the longer half-life of ^{18}F, Serdons et al. developed another series of ^{18}F-labeled BTAs by moving the ^{18}F atom to the 4′-position (Table 3, **21**–**27**) [46–48]. Scheme 1, approach B and C were applied to prepare the BTA core for these ligands. Except for **23** (R_1 = OH, $K_i = 22.5$ nM), all the rest ligands showed high binding abilities to human AD brain homogenates ($K_i \leq 10$ nM), which were comparable to that of PIB ($K_i = 2.8$ nM) in the identical assay. Among them, ligands **25** possessed the highest initial brain uptake (13.97 %ID/g at 2 min) and rapid washout from normal regions with $brain_{2\ min}/brain_{60\ min}$ ratio of 14.4, which were much better than [^{11}C]PIB in the same assay. However, μPET study with [^{18}F]**25** in a normal rhesus monkey showed slightly higher non-specific background binding than [^{11}C]PIB. Thereafter, Lee et al. reported three radiofluorinated BTA analogs with ^{18}F atom incorporating at 6-position (Table 3, **28**–**30**) [49]. The BTA backbone was simply obtained from substituted 2-aminobenzenethiol and benzaldehyde in DMSO at 180 °C (Scheme 1, Approach B). As the general aromatic fluoride ion substitution with a nitro group failed to effect ^{18}F labeling at the 6-position, an alternative pathway using diaryliodonium tosylate salts as precursors was adopted. The diaryliodonium tosylate precursors were prepared by reaction of 6-tributyltin compounds with a commercially available hydroxy(tosyloxy)iodobenzene (Koser's reagent) or various hydroxy(tosyloxy)iodoarenes. In the radiosynthesis of these compounds, aromatic radiofluorination using cesium [^{18}F]fluoride or potassium [^{18}F]fluoride/kryptofix 2.2.2 as radiofluorinating agents did not work, while n-butylammonium [^{18}F]fluoride was proved to be more efficient. These low radiochemical yields might be attributable to the radical-induced decomposition of diaryliodonium tosylate salts in a base condition, thus a radical scavenger, 2,2,6,6-tetramethylpiperidinel-oxyl

Table 8
Binding affinities and brain pharmacokinetics of ^{99m}Tc-labeled 2-pehnylbenzoxazole derivatives **72** and **73**.

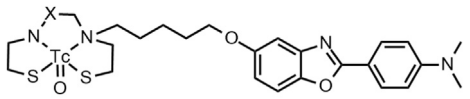

Compound	$A\beta_{42}$ K_i (nM)	Brain uptake (%ID/g)		Ref.
		2 min	60 min	
72	11.1	0.81	0.25	[77]
73	14.3	0.43	0.30	[77]

Table 9
Binding affinities and brain pharmacokinetics of 2-arylbenzofuran derivatives **74**–**84**.

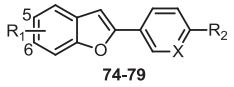

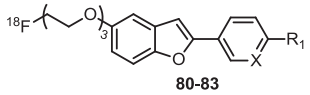

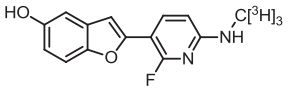
[^{3}H]**84**: AZD4694

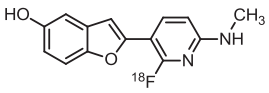
[^{18}F]**84**: AZD4694

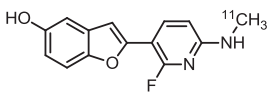
[^{11}C]**84**: AZD4694

Compound	R_1	R_2	X	Aβ_{40} K_i (nM)	Brain uptake (%ID/g)		Ref.
					2 min	60 min	
74	5-^{125}I	NMe_2	CH	7.7	0.51[a]	1.08[a]	[78]
75	5-^{125}I	NHMe	CH	1.1	0.78[a]	1.20[a]	[78]
76	6-^{125}I	NMe_2	CH	0.4	0.48[a]	1.00[a]	[78]
77	5-^{125}I	OH	CH	6.5	1.40[a]	1.51[a]	[78]
78	5-^{125}I/^{123}I	NHMe	N	2.94[b]	4.17	1.30	[80]
79	5-OH	NH$^{11}CH_3$	CH	0.7[c]	4.78	0.19	[81]
80 (FPHBF-1)	NMe_2	–	CH	2.0[b]	2.88	2.80	[82]
81 (FPYBF-1)	NMe_2	–	N	0.9[b]	5.16	2.44	[83]
82 (FPHBF-2)	NHMe	–	CH	3.85[b]	8.18	3.87	[84]
83 (FPYBF-2)	NHMe	–	N	2.41[b]	7.38	3.15	[84]
84 (AZD4694)	–	–	–	2.3[d]	–	–	[85]

[a] Expressed as %ID/organ in normal mice.
[b] Expressed as K_i for Aβ_{42} aggregates.
[c] Expressed as binding to amyloid plaques in human AD brain homogenates.
[d] Expressed as K_d for Aβ_{40} aggregates.

(TEMPO), was added to stabilize the diaryliodonium tosylate salts, increasing the radiochemical yields significantly. The fluorine-18 anion attacked the more electron deficient benzothiazole ring of these precursors, offering [^{18}F]**28**–**30** in radiochemical yields of 19–40%. One of these probes, [^{18}F]**29** exhibited good binding affinity to Aβ_{40} aggregates (K_i = 5.5 nM), highest rate of brain uptake (6.62 %ID/g at 2 min) and fastest brain washout ($brain_{2\ min}$/$brain_{60\ min}$ = 9.07).

Over the last decade, several PET imaging agents have been conducted in AD patients in clinical trials, but are still limited to the minority of modern hospitals equipped with PET scanners. As SPECT is more widely valuable than PET, great effort has been directed toward the development of SPECT imaging agents for visualization of Aβ plaques. In view of the nearly optimal nuclear and imaging properties (E_γ = 141 keV, $t_{1/2}$ = 6.01 h) and easy access with a commercial ^{99}Mo/^{99m}Tc generator, technetium-99m is the most widely used radionuclide for SPECT imaging. Thus several ^{99m}Tc-labeled 2-phenylbenzothiazole derivatives have been synthesized and screened for SPECT imaging of Aβ plaques (Table 4, **31**–**38**) [50–54]. As the lead 2-phenylbenzothiazole core does not contain sufficient donor atoms for metal-binding, metal ^{99m}Tc was incorporated through a conjugated approach by linking the amyloid-binding molecule to various bifunctional chelating ligands (BCLs) including bisamine-bisthiol (BAT), monoamine-monoamide bisthiol (MAMA), mercaptoacetyltriglycine (MAG3), hydrazino nicotinic acid (HYNIC), iminodiacetic acid (IDA) and 2-((pyridin-2-ylmethyl)amino)acetic acid (PMAA). Unfortunately, these ^{99m}Tc labeled complexes failed to cross the BBB to a sufficient degree and thus were not capable of detecting Aβ deposits in vivo. This may be due to the large molecular size or ionized nature at physiological pH. Among them, **32** displayed highest initial brain uptake (1.34 %ID/g at 2 min) but delayed clearance with $brain_{2\ min/60\ min}$ ratio as low as 2.4. In addition, its blood background was high (4.43 %ID/g at 60 min), which was an unfavorable factor for imaging applications [51].

Besides the well-studied BTA analogs, several other benzothiazole scaffolds (Table 5) have been designed and evaluated to visualize the Aβ plaques. This would probably extend the chemical library of Aβ probes. Wu et al. synthesized a ^{125}I-labeled dibenzothiazole (Table 5, **39**) through two steps of coupling between 2-aminothiophenols and corresponding benzoyl chlorides (Scheme 1, Approach B) [55]. It exhibited moderate binding ability (K_i = 21 nM) and brain uptake (3.71 %ID/g at 2 min). Two ^{125}I-labeled bithiophene benzothiazoles (Table 5, **40**–**41**) have been developed by condensation of 2-aminothiophenols and [2,2′-bithiophene]-5-carbaldehydes (Scheme 1, Approach B) [56]. Both ligands showed high binding affinities to Aβ aggregates and good in vitro labeling of Aβ deposits on brain sections from transgenic mice. Surprisingly, appending the ^{125}I atom to the thiophene ring (**41**) resulted in much less favorable brain pharmacokinetics (0.87 % ID/g at 2 min). In vitro stability in liver homogenate showed that **41** underwent severe deiodination in liver, which may be caused by oxidation of the adjacent sulfur atom. Thereafter, a series of ^{125}I- and ^{18}F-labeled phenyldiazenyl benzothiazoles (Table 5, **42**–**45**) were investigated as neurofibrillary tangles (NFTs) imaging candidates by Matsumura et al., but they possessed high affinity for both tau and Aβ aggregates [57,58]. As these ligands showed rather low uptake and slow washout in the normal mice brain, further modifications may be necessary to improve the binding selectivity and brain pharmacokinetics. Recently, Gan and his coworkers synthesized a group of benzothiazole schiff-bases (Table 5, **46**–**51**) by direct condensation of 2-amino-5-methoxybenzothiazole and different benzaldehyde under the catalysis of acetic acid [59]. These compounds showed high to low binding affinities for AD brain homogenates (K_i = 4.38–514.65 nM), depending on the substitution on the phenyl ring. However, radiolabeling and in vivo studies were not conducted.

4. Benzoxazole derivatives

Replacing the sulfur atom of the benzothiazole core by its bioisostere, oxygen, generated the benzoxazole scaffold. The first reported benzoxazole derivative [^{125}I]IBOX (Table 6, **52**) was

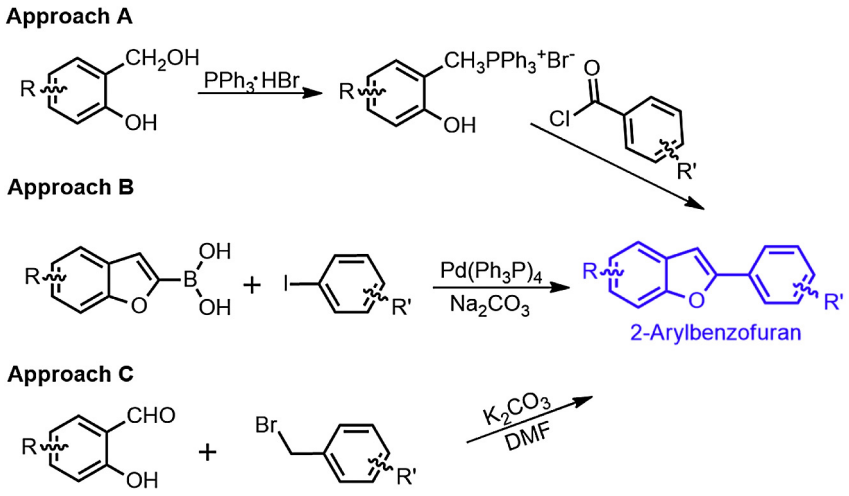

Scheme 3. General synthetic approaches to the 2-arylbenzofuran core.

synthesized via a condensation reaction between 5-nitro-2-aminophenol and 4-dimethylaminobenzoic acid catalyzed by boric acid (Scheme 2, Approach A) [60,61]. Comparing with the benzothiazole compound [^{125}I]TZDM (Table 1, **7**), [^{125}I]IBOX displayed similar binding potency to Aβ_{40} aggregates (K_i = 0.8 nM), superior peak brain uptake (2.08 %ID at 30 min) and faster clearance in normal mice. Expanding on this 2-phenylbenzoxazole, Hausner et al. synthesized a class of 5- and 6-aromatic amide substituted benzoxazoles through the boric acid catalyzed condensation mentioned above [62]. Several of these compounds showed high binding affinities with K_i values range in the low-nanomolar degree, the most promising **53** was selected for ^{123}I-radiolabeling and SPECT imaging in a baboon model. Things went athwart, [^{123}I]**53** did not cross the BBB to any significant extent, and this may be attributed to its excessively high lipophilicity (*C*Log *P* 6.11). To reduce the lipophilicity and non-specific binding, a class of 2-pyridylbenzoxazoles were synthesized and evaluated as PET imaging agents (Table 6, **54**–**57**) targeting to Aβ plaques [63,64]. The 2-arylbenzoxazole backbone was obtained via an oxidative cyclization of a phenolic Schiff base, derived from the condensation of 2-aminophenols and related formylpyridines, using versatile 2,3-dichloro-5,6-dicyano-1,4-benzoquinone (DDQ) as oxidant (Scheme 2, Approach C) [65]. Although a decline in binding affinities was observed, [^{3}H]**54** exhibited increased signal-to-background ratios in autoradiographic studies in vitro and ex vivo in APP/PS1 mice. Then Cui et al. applied the pegylation-fluorination strategy to benzoxazole scaffold, resulting in a group of fluoropegylated 2-phenylbenzoxazole (**58**–**59**) and 2-pyridinylbenzoxazole (**60**–**63**) derivatives to light up the Aβ deposites in AD brain [39,66]. Polyphosphoric acid (PPA) catalyzed condensation of 2-amino-4-methoxyphenol and corresponding benzoic acids successfully afforded the desired 2-phenylbenzoxazole core (Scheme 2, Approach A). In the preparation of the 2-pyridinylbenzoxazole backbone, an alternative condensation with anionically activated 2-amino-5-(trifluoromethyl)pyridine under a mild aqueous condition (NaOH, 1 M) was adopted (Scheme 2, Approach B), and the yield was improved up to 89% [20]. All the ligands showed high binding potency to Aβ_{42} aggregates (K_i = 2.7–9.9 nM) except for **60**. Ligands **62** and **63** with a short length of FPEG chain (n = 1) exhibited most favorable initial uptake ($\geq$7 %ID/g at 2 min) and rapid washout ($brain_{2\ min}$/$brain_{60\ min}$ ratio $\geq$ 4.5) from the brain. Besides, ex vivo autoradiography studies with [^{18}F]**62** showed clear labeling of Aβ deposits in the cortical regions of APP/PS1 mice.

Okamura and his coworkers designed and examined a series of styrylbenzoxazole derivatives by introducing a double bond between the benzoxazole and phenyl ring, and two of these compounds (Table 7, **64**–**65**) achieved high binding affinities for Aβ_{42} aggregates (K_i = 4.4 and 3.9 nM, respectively) and distinctively recognized compact and diffuse plaques in AD brain sections [67–69]. A convenient one-step PPSE (polyphosphoric acid trimethylsilyl ester) catalyzed condensation of 2-aminophenols and relate cinnamic acids successfully afforded the styrylbenzoxazole backbone (Scheme 2, Approach D). While compound **65** was synthesized through a more complex pathway: a LDA (lithium diisopropylamide) promoted reaction between 6-methoxy-2-methylbenzo[d]oxazole and tert-butyl (4-formylphenyl) (methyl) carbamate followed by a dehydration using MsCl and Et_3N (Scheme 2, Approach E) [69]. Further structural modification by replacing the phenyl ring with a thiazole ring generated another class of benzoxazole derivatives (Table 7, **66**–**67**), of witch [^{11}C]BF-227 (**66**) displayed high binding affinity (K_i = 4.3 nM) and excellent in vivo brain pharmacokinetics (7.9 %ID/g at 2 min and 0.64 % ID/g at 60 min) [70–73]. Clinical [^{11}C]BF-227 PET results in AD patients showed significantly higher uptake and retention than aged normal controls in the bilateral temporoparietal region containing a high level of plaques. Additional PET studies with [^{11}C]BF-227 demonstrated its potency to distinctly differentiate AD and mild cognitive impairment (MCI) patients from healthy control groups [74]. However, high levels of retention of this agent in white matter and thalamic were observed. In an effort to reduce non-specific binding, Harrison et al. reported a group of less lipophilic oxazolo[5,4-*b*]pyridine derivatives (Table 7, **68**–**71**) to assess the Aβ plaques load in the brain [75]. A reaction between 2-fluoropyridin-3-amines and corresponding Ghosez' reagent activated aromatic acids in pyridine afforded the intermediate amides. Following microwave heating of the amides with K_2CO_3 or Cs_2CO_3 in DMF successfully provided the key azabenzoxazole scaffold (Scheme 2, Approach F) [76]. [^{18}F]MK-3328 (**68**) exhibited the most promising combination of high affinity for human amyloid plaques (IC_{50} = 10.5 nM) and high brain uptake with low binding potential in white matter and cortical gray matter. [^{18}F]MK-3328 is currently under Phase III clinical trials.

The benzoxazole scaffold was also ^{99m}Tc labeled by coupling MAMA and BAT chelating ligands via a pentyloxy spacer (Table 8, **72** and **73**) [77]. Both compounds showed high affinity for Aβ_{42} aggregates (K_i = 11.1 nM and 14.3 nM, respectively) and clearly labeled amyloid deposits on transgenic mouse brain sections.

Table 10
Binding affinities and brain pharmacokinetics of ^{99m}Tc-labeled 2-arylbenzofuran derivatives **85**–**89**.

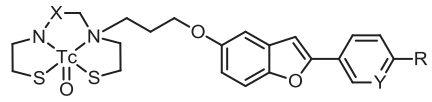

85-89

Compound	R	X	Y	Aβ_{42} K_i (nM)	Brain uptake (%ID/g)		Ref.
					2 min	60 min	
85	NMe_2	CH_2	CH	11.5	1.34	0.56	[89]
86	NMe_2	CO	CH	24.4	0.74	0.89	[89]
87	NH_2	CH_2	N	149.6	1.59	0.97	[90]
88	NHMe	CH_2	N	32.8	1.80	0.79	[90]
89	NMe_2	CH_2	N	13.6	1.41	0.79	[90]

Table 11
Binding affinities and brain pharmacokinetics of benzothiophene derivatives **90**–**91**.

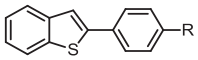

90-91

Compound	R	Aβ_{42} K_i (nM)	Brain uptake (%ID/g)		Ref.
			2 min	30 min	
90	$OEt^{18}F$	0.87	5.2	5.2	[91]
91	$OPr^{18}F$	0.73	3.3	4.0	[91]

Table 12
Binding affinities and brain pharmacokinetics of indole derivatives **92**–**99**.

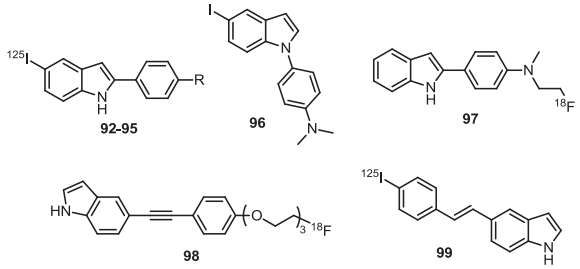

92-95 **96** **97** **98** **99**

Compound	R	Aβ_{42} K_i (nM)	Brain uptake (%ID/g)		Ref.
			2 min	60 min	
92	NHMe	27.0	1.10	0.83	[92]
93	NMe_2	4.24	1.19	0.71	[92]
94	OMe	20.2	2.11	1.16	[92]
95	OEtOH	25.9	2.13	1.82	[92]
96	–	>10,000	–	–	[92]
97	–	28.4	5.82	2.77	[95]
98	–	1.5	2.43	2.10[a]	[97]
99	–	4.1[b]	4.27	0.28	[98]

[a] Expressed as brain uptake at 3 h post-injection.
[b] Expressed as K_i for Aβ_{40} aggregates.

However, the brain uptake levels were too low to satisfy the imaging requisite for brain (0.81 and 0.43 %ID/g at 2 min).

5. Benzofuran derivatives

Isosteric replacement of the heterocyclic nitrogen atom in benzoxazole core by a CH group leaded to the benzofuran scaffold target to Aβ plaques. In 2002, Ono et al. first synthesized a series of ^{125}I-labeled benzofuran derivatives (Table 9, **74**–**77**) through an intramolecular Wittig reaction between triphenyl phosphonium salts and 4-substituted benzoyl chlorides (Scheme 3, Approach A) [78,79]. And the Wittig reagent triphenyl phosphonium salt was prepared via a one-pot conversion of the substituted benzyl alcohol to benzyl bromide followed by reaction with triphenylphosphine. These ^{125}I-labeled compounds showed excellent binding to Aβ_{40} aggregates with K_i values in the subnanomolar range, but unfavorable clearance from normal brain indicating high non-specific binding. Thereafter, a ^{123}I-labeled less lipophilic 2-pyridylbenzofuran derivative (**78**) was evaluated as SPECT imaging agent for visualizing Aβ plaques [80]. The key 2-pyridylbenzofuran backbone was formed with a Suzuki coupling reaction between (5-bromobenzofuran-2-yl)boronic acid and 5-iodo-N-methylpyridin-2-amine (Scheme 3, Approach B). [^{125}I]**78** possessed strong binding to Aβ_{42} aggregates (K_i = 2.94 nM) and moderate brain uptake and washout rate. SPECT/CT with [^{123}I]**78** revealed significant difference in radioactivity accumulation in the Tg2576 mouse brain and the wild-type mouse brain. In an attempt to explore the ligands for PET, a ^{11}C-labeled 2-phenylbenzofuran derivative (**79**) was developed through the intramolecular Wittig reaction mentioned above (Scheme 3, Approach A) [81]. The washout rate was increased with $brain_{2\ min}/brain_{60\ min}$ ratio as high as 25.

Searching for ^{18}F-labeled compounds with improved in vivo properties, four fluoro-pegylated benzoxazole derivatives (**80**–**83**) were investigated by the same authors [82–84]. FPHBF-1 (**80**) was synthesized through the intramolecular Wittig reaction (Scheme 3, Approach A), while FPYBF-1 (**81**) and FPYBF-2 (**83**) were constructed via the Suzuki coupling (Scheme 3, Approach B). In contrast, the backbone of FPHBF-2 (**82**) was formed by a base-promoted condensation of 2-hydroxy-5-methoxybenzaldehyde and 1-(bromomethyl)-4-nitrobenzene (Scheme 3, Approach C). All of them displayed excellent binding to Aβ aggregates (K_i = 0.9–3.85 nM) and clearly visualized the Aβ plaques in Tg2576 mice brains by ex vivo autoradiography. The monomethylamino group substituted FPHBF-2 and FPYBF-2 showed higher brain uptakes (8.18 and 7.38 %ID/g at 2 min) but still unfavorable clearance profile ($brain_{2\ min}/brian_{60\ min}$ ratio < 2.5). A ^{3}H-labeled fluorinated pyridylpbenzoxazole (AZD4694, **84**) also showed promise properties for amyloid imaging (K_d = 2.3 nM). Compared with [^{3}H]flutemetamol and [^{3}H]PIB, [^{3}H]AZD4694 selectively labeled plaques in gray matter with the lowest level of non-specific binding in plaque devoid white matter [85]. Clinical PET examinations with [^{18}F]AZD4694 showed rapid brain entrance, reversible specific binding

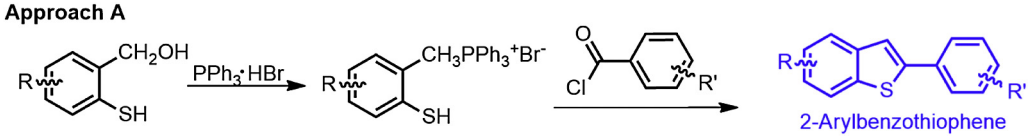

Scheme 4. Synthetic strategy to the 2-arylbenzothiophene core.

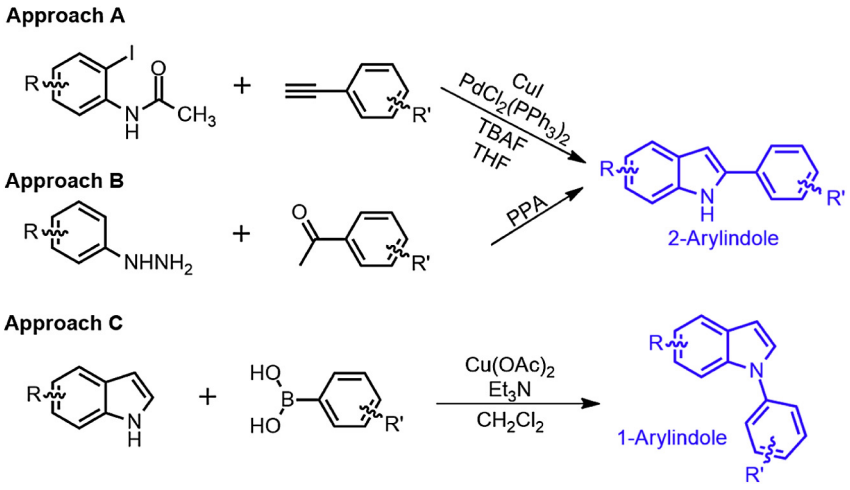

Scheme 5. General synthetic approaches to the indole core.

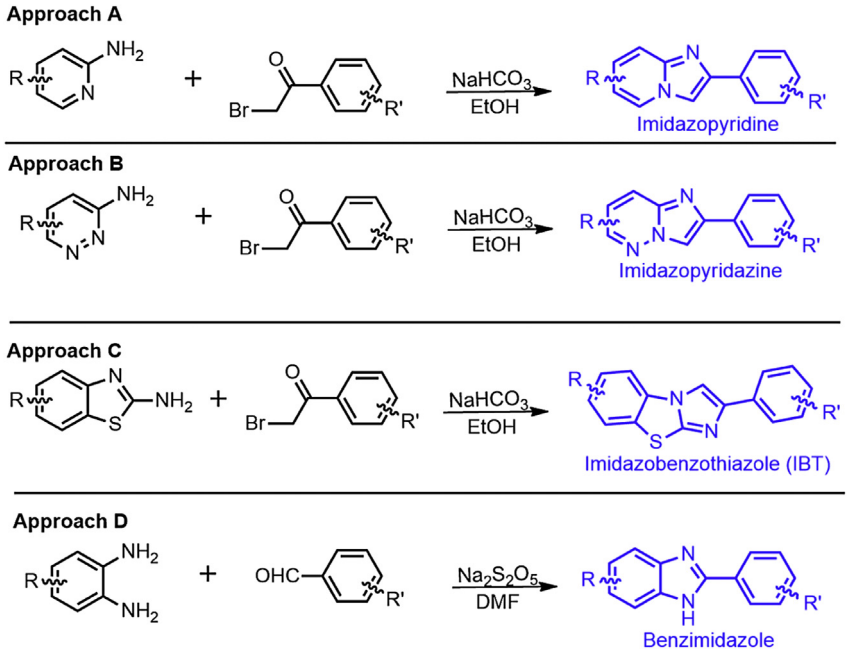

Scheme 6. General synthetic approaches to the imidazopyridine, imidazopyridazine, imidazobenzothiazole and benzoimidazole core.

and significantly low white matter binding nearly identical to those of [^{11}C]PIB [86,87]. [^{18}F]AZD4694 is now under Phase II clinical trials. Recently, ^{11}C-labeld AZD4694 was prepared in a high radiochemical yield and in vivo evaluated in nonhuman primates. [^{11}C]AZD4694 displayed rapid brain pharmacokinetics as well as slightly lower non-specific binding in white matter than [^{11}C]PIB [88].

Building on the promising 2-arylbenzofuran scaffold, several ^{99m}Tc/Re complexes (Table 10, **85**–**89**) using BAT and MAMA as the chelating ligands were studied for Aβ imaging [89,90]. The formation of the benzofuran core was readily achieved by base-promoted condensation for **85**–**86** (Scheme 3, Approach C) and Suzuki coupling (Scheme 3, Approach B) for **87**–**89**. These ^{99m}Tc complexes displayed decreased binding affinities (K_i = 11.5–149.6 nM) than other benzofuran derivatives discussed above, which can be attributed to the introduction of the big chelating ligands. Among these probes, [^{99m}Tc]**88** possessed highest brain uptake (1.80% ID/g at 2 min) and a reasonable washout from the brain. In addition, ex vivo autoradiographic results showed intensive labeling of amyloid plaques in the transgenic mice brains.

6. Benzothiophene derivatives

Based on the advantages of benzofuran derivatives, a series of benzothiophene derivatives (Table 11, **90**–**91**) were also investigated as novel Aβ imaging probes [91]. Once again, the intramolecular Wittig reaction was applied to prepare the benzothiophene backbone from triphenyl phosphonium salts and 4-substituted benzoyl chlorides in good yields (Scheme 4). Both compounds showed excellent binding to Aβ_{42} aggregates (K_i = 0.87 and 0.73 nM), but poor brain clearance profiles ($brain_{2\ min}$/$brain_{30\ min}$ ratios $\leq$ 1) due to the increased lipophilicity by replacing the oxygen with a sulfur atom. Thus, at present no more ligands based on benzothiophene scaffold have been reported.

Table 13
Binding affinities and brain pharmacokinetics of imidazopyridine, imidazopyridazine and benzoimidazole derivatives **100**–**111**.

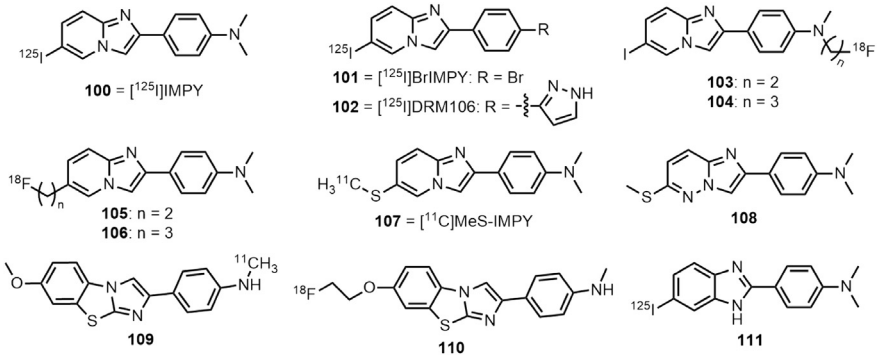

Compound	$A\beta_{40}$ K_i (nM)	Brain uptake (%ID/g)		Ref.
		2 min	60 min	
100 (IMPY)	15	2.88[a]	0.21[a]	[100]
101 (BrIMPY)	7.48[b]	–	–	[105]
102 (DRM106)	1.86[c]	0.45[d]	0.02[d]	[106]
103 (FEM-IMPY)	27	6.4[e]	4.5[f]	[107]
104 (FPM-IMPY)	40	5.7[e]	2.1[f]	[107]
105 (FEPIP)	177[g]	–	–	[108]
106 (FPPIP)	48.3[g]	–	–	[108]
107 (MeS-IMPY)	7.93[g]	–	–	[109]
108	11.0	–	–	[110]
109	3.5	9.2[h]	1.1[i]	[112]
110	2.1	7.2[h]	1.2[i]	[113]
111	9.8[b]	4.14	0.15	[114]

[a] Expressed as %ID/organ in normal mice.
[b] Expressed as K_i for $A\beta_{42}$ aggregates.
[c] Expressed as IC_{50} for $A\beta_{40}$ aggregates.
[d] Expressed as %ID/g in normal rats.
[e] Expressed as high uptakes in PET experiments with normal mice.
[f] Expressed as brain uptake at 2 h post-injection.
[g] Expressed as K_i for human AD brain homogenates.
[h] Expressed as brain uptake at 5 min post-injection.
[i] Expressed as brain uptake at 30 min post-injection.

7. Indole derivatives

Watanabe et al. developed a series of ^{125}I-labeled phenylindole derivatives (Table 12, **92**–**96**) for amyloid imaging [92]. The 2-phenylindole backbone was prepared by a one-pot, two-step Sonogashira reaction and cyclization reaction of 2-iodoanilines and terminal alkynes using a palladium catalyst in the presence of tetrabutylammonium fluoride (TBAF) in yields of 27.2–49.5% (Scheme 5, Approach A) [93]. The phenyl ring was also attached to the 1-position of the indole ring via a copper-mediated coupling of substituted indole with substituted phenylboronic acid (Scheme 5, Approach C) [94]. This strategy expanded the use of boronic acids in formation of carbon-heteroatom bonds. The 2-phenylindole derivatives **92**–**95** exhibited good inhibitory activities toward $A\beta$ aggregates (K_i = 4.24–27.0 nM), while the N-substituted indole **96** did not (K_i > 10,000). However, the low uptake and slow washout from normal brain made them unsuitable for brain imaging. Thereafter, a fluorinated 2-phenylindole derivative (Table 12, **97**) was also investigated to label $A\beta$ deposits in the brain by Fu et al. [95]. The classic Fischer indole synthesis strategy was applied to prepare the 2-phenylindole scaffold from 1-(4-(methylamino)phenyl)ethanone and phenylhydrazine in the presence of PPA [96]. [^{18}F]**97** showed intense and specific labeling of $A\beta$ plaques in in vitro autoradiographic studies and increased uptake into brain (5.82 %ID/g at 2 min) but moderate washout. Qu et al. prepared a fluoro-pegylated indolylphenylacetylene (Table 12, **98**) which displayed good binding affinity but unfavorable brain uptake and clearance property (2.43 %ID/g at 2 min and 2.10 %ID/g at 3 h) [97]. To fine-tune the brain pharmacokinetics, Yang et al. developed a ^{125}I-labeled styrylindole (**99**) with combination of high binding activity (K_i = 4.1 nM) and high initial brain uptake followed by rapid clearance from normal brain ($brain_{2\ min}/brain_{60\ min}$ = 15) [98].

8. Imidazopyridine, imidazopyridazine and benzoimidazole derivatives

Searching to improve the brain kinetics and lower the non-specific binding, Kung et al. first reported a series of imidazo[1,2-*a*]pyridine derivatives as novel $A\beta$-specific ligands [99–103]. The imidazo[1,2-*a*]pyridine ring was readily formed by a fusion reaction between α-bromoacetophenone and 2-aminopyridine under a mild basic condition (Scheme 6, Approach A). One of the most promising compound, IMPY (Table 13, **100**), exhibited a good binding to $A\beta_{40}$ aggregates (K_i = 15 nM) and distinct plaque labeling in ex vivo autoradiograms of the Tg2576 mouse brain sections. Biodistribution study of [^{125}I]IMPY showed much-improved brain uptake (2.9 %ID/brain at 2 min) and rapid washout (0.2 %ID/brain at 60 min), indicating a low background activity. Then IMPY was ^{123}I labeled and evaluated in AD patients and cognitively normal control subjects. It appears to be pharmacologically safe in vivo, but the

Table 14
Binding affinities and brain pharmacokinetics of quinoline derivatives **112**–**118**.

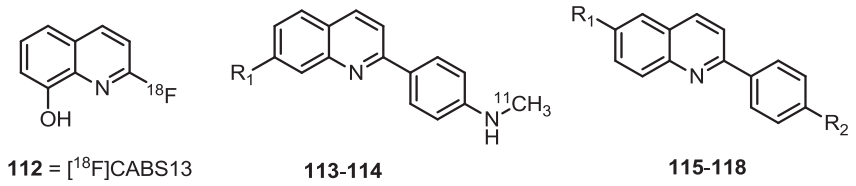

112 = [^{18}F]CABS13 **113-114** **115-118**

Compound	R_1	R_2	Tau K_i (nM)	Brain uptake (%ID/g)		Ref.
				2 min	30 min	
112 (CABS13)	–	–	1.5[a]	10	1.1	[115]
113 (BF-158)	H	–	399[b]	11.3	3.1	[116]
114 (THK-951)	OH	–	20.7	3.23	0.11	[117]
115 (THK-523)	OEt^{18}F	NH_2	1.67[c]	2.75	–	[118]
116 (THK-5105)	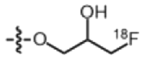	NMe_2	7.8	9.20	1.00	[119]
117 (THK-5116)	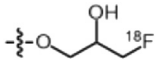	NH_2	36.0	3.36	0.57	[119]
118 (THK-5117)	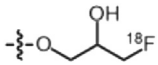	NHMe	10.5	6.06	0.26	[119]

[a] Expressed as K_d for Aβ–Zn aggregates.
[b] Expressed as IC_{50} for tau fibrils.
[c] Expressed as K_d for tau fibrils.

signal-to-noise ratio for plaque labeling was not satisfactory, preventing its clinical translation. And this low contrast was attributed to the in vivo instability and rapid metabolism [104]. The proposed metabolic mechanism was mainly enzyme-catalyzed N-demethylation, then a series of various functional groups substituted IMPYs were synthesized and evaluated directing at improving the in vivo metabolic stability [105,106]. Among them, ligands with 4′-bromo (BrIMPY, **101**) and 4′-pyrazole substituent (DRM106, **102**) exhibited combined high binding affinities for Aβ and high in vivo metabolic stability. The half-life of [^{125}I]IMPY in samples of brain homogenates was shorter than 3 min, while that of [^{125}I]BrIMPY was longer than 60 min [105]. Metabolic analysis of [^{125}I]DRM106 by radio-TLC clearly demonstrated that no detectable metabolites existed in the brain over 8 h [106]. To develop novel ligands for PET amyloid imaging using the core structure of IMPY, Cai et al. synthesized two ^{18}F-labeled imidazo[1,2-*a*]pyridine derivatives (**103**–**104**) by replacing the N-methyl group of IMPY with a 2-fluoroethyl or 3-fluoropropyl group [107]. In which the imidazo[1,2-*a*]pyridine was obtain by the mild base promoted condensation discussed above (Scheme 6, Approach A). Compared with the parent IMPY, these two compounds displayed lower binding potencies and slower biphasic clearances. In addition, metabolism results indicated severe dealkylation of the tertiary arylamino group and defluorination, resulting in the trapping of polar metabolites in the brain and uptake of [^{18}F]fluoride in the skull. Replacement of the iodine atom of IMPY with a fluoroethyl and fluoropropyl group generated another two fluorinated imidazo[1,2-*a*]pyridine derivatives (**105**–**106**) [108]. Micro-PET imaging with [^{18}F]FPPIP (**106**)

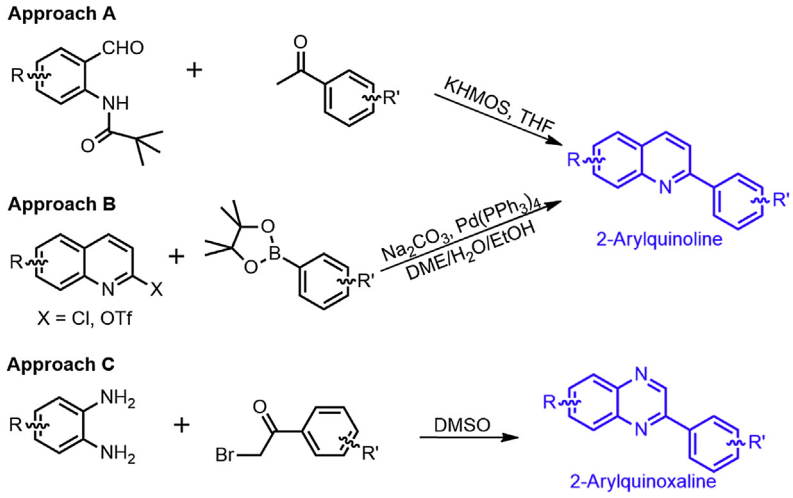

Scheme 7. General synthetic approachs to the 2-arylquinoline and 2-arylquinoxaline scaffolds.

Table 15
Binding affinities and brain pharmacokinetics of quinoxaline derivatives **119**–**127**.

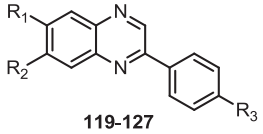

119-127

Compound	R_1	R_2	R_3	$A\beta_{42}$ K_i (nM)	Brain uptake (%ID/g)		Ref.
					2 min	60 min	
119	^{125}I	H	NMe_2	4.1	6.03	2.91	[120]
120	NHMe	H	$OEt^{18}F$	10.0	8.17	3.17	[121]
121	NHMe	H	$(OEt)_3^{18}F$	5.3	2.49	0.64	[121]
122	H	$OEt^{18}F$	NH_2	1180	4.69	1.99	[122]
123	H	$OEt^{18}F$	NHMe	758	5.96	1.91	[122]
124	H	$OEt^{18}F$	NMe_2	111	5.78	1.48	[122]
125	$OEt^{18}F$	H	NH_2	242	7.59	3.08	[122]
126	$OEt^{18}F$	H	NHMe	15.7	6.19	2.41	[122]
127	$OEt^{18}F$	H	NMe_2	0.895	5.67	2.61	[122]

in a rhesus monkey indicated easy brain entry, relatively fast non-specific binding clearance and low in vivo defluorination. However, more structural refinement is required to increase binding affinity. Seneca et al. also investigated a ^{11}C-labeled IMPY analog (**107**) as a potential radiotracer for imaging Aβ plaques with PET [109]. [^{11}C]MeS-IMPY showed a good binding affinity (K_i = 7.93 nM) comparable to IMPY (K_i = 8.95 nM), high brain uptake, fast clearance and quantifiable volume of distribution in nonhuman primate brain.

In an attempt to reduce the lipophilicity, Zeng et al. developed a class of isosteric analogs of IMPY, imidazo[1,2-*b*]-pyridazines, by replacing the pyridine ring with pyridazine ring [110]. Once again, the mild base promoted fusion condensation proved to be a suitable approach to prepare the imidazo[1,2-*b*]-pyridazine ring from α-bromoacetophenones and 3-amino-6-halopyridazines (Scheme 6, Approach B). It is worth mentioning that the introduction of a halogen in the pyridazine ring played a key role in the successful formation of imidazo[1,2-*b*]pyridazine core in good yields. Following nucleophilic substitution of the 6-halo derivatives afforded compounds bearing various substituent on the 6-position. These compounds showed various binding affinities range from 11.0 to >1000 nM. The 6-methylthio analog **108** (K_i = 11.0 nM) seems to be interest for evaluation as a promising PET candidate by labeling with carbon-11 on the N-methyl or S-methyl position, but radiolabeling and in vivo studies were not reported.

Alagille et al. reported a small group of mix-condensed analogs of the two most potent Aβ imaging agents, PIB and IMPY. These imidazo[2,1-*b*]benzothiazoles (IBTs) bearing various hydrogen bond donating and accepting substituents displayed acceptable binding affinity for Aβ_{40} aggregates, ranging from 6 to 133 nM [111]. Almost at the same time, another research group designed and synthesized several ^{11}C- and ^{18}F-labeled IBTs [112,113]. Similar to the preparation of the imidazopyridine and imidazopyridazine, the IBT core was built by the same fusion condensation with the use of 2-aminobenzothiazole instead of 2-aminopyridine (Scheme 6, Approach C). Among these compounds, [^{11}C]**109** and [^{18}F]**110** possessed combined favorable properties of high in vitro affinity for Aβ aggregates, suitable brain entry/clearance kinetics and high metabolic stability in the brain. Small-animal PET studies revealed that [^{11}C]**109** and [^{18}F]**110** bound to Aβ plaques in the brain of APP/PS1 mice in a comparable binding pattern with [^{3}H]PIB.

In 2001, Cui et al. synthesized several iodinated 2-phenyl-1H-benzo[d]imidazole (BZMZ) derivatives by an intermolecular cyclization between substituted benzene-1,2-diamines and benzaldehydes using $Na_2S_2O_5$ as an oxidant (Scheme 6, Approach D) [114]. The N,N-dimethylamino substituted ligand **111** showed highest affinity (K_i = 9.8 nM) and moderate brain entry followed by fast washout from normal brain ($brain_{2\ min}/brain_{60\ min}$ = 27.6). In addition, [^{125}I]**111** selectively labeled the Aβ plaques in vivo in an AD transgenic mice and in vitro in AD human brain sections.

9. Quinoline and quinoxaline derivatives

The Aβ imaging agents discussed above mainly consist of a benzene fused five-membered heterocyclic ring system. Enlargement of the five-membered heterocyclic ring resulted in a series of quinoline and quinoxaline derivatives for visualizing the Aβ plaques. Vasdev et al. developed a [^{18}F]2-fluoroquinolin-8-ol ([^{18}F]CABS13, **112**) with excellent binding to Aβ–Zn aggregates (K_d = 1.5 nM) [115]. PET-CT imaging studies revealed significantly higher retention of [^{18}F]CABS13 (**112**) in transgenic mouse brains than wild-type controls. In contrast, several other 2-arylquinoline derivatives (Table 14, **113**–**118**) showed high binding affinity and selectivity for tau fibrils over Aβ plaques [116–119]. The 2-arylquinoline backbone was synthesized through a cyclo-condensation reaction of benzaldehyde and acetophenone in the presence of potassium bis(trimethylsilyl)amide (KHMOS) (Scheme 7, Approach A) [117]. The substituted 2-chloroquinoline and quinoline triflate were also used for the preparation of 2-arylquinoline core via a Suzuki coupling reaction with corresponding boronic acid pinacol esters (Scheme 7, Approach B) [117]. Preclinical examination demonstrated that [^{18}F]THK-523 (**114**) was able to selectively highlight tau pathology in the brain both in vitro and in vivo [118]. Introducing another N atom into the heterocyclic ring led to a series of 2-arylquinoxaline derivatives, which were expected to be less lipophilic. The 2-phenylquinoxaline core was constructed via a one-pot tandem oxide condensation of *a*-bromoacetophenone and substituted *o*-phenylenediamines (Scheme 7, Approach C) [120]. These quinoxaline analogs exhibited excellent binding to Aβ_{42} aggregates with K_i values ranging from 2.6 to 10.7 nM, which were comparable to that of IMPY. The tertiary N,N-dimethylamino derivative **119** was ^{125}I labeled and it showed a high uptake (6.03% ID/g at 2 min) into but a slow washout from the brain. Thereafter, the same research group developed two fluoropegylated quinoxaline derivatives (Table 15, **120**–**121**) possessing good binding potencies to Aβ_{42} aggregates (K_i = 10.0 and 5.3 nM, respectively) [121]. The specific binding was confirmed by in vitro autoradiography on AD human and APP/PS1 mouse brain sections. Ligand [^{18}F]**120** with a short length of FPEG chain (n = 1) displayed much higher initial brain uptake (8.17 %ID/g at 2 min) followed by moderate clearance. Then Yoshimura et al. described the structure–activity relationships (SAR) and in vivo evaluation of a new class of ^{18}F-labeled quinoxaline derivatives (**122**–**127**) for PET imaging of Aβ plaques. Obviously, the 6-fluoropegylated derivatives exhibited much higher affinities (K_i = 0.895–242 nM) than corresponding 7-fluoropegylated ones (K_i = 111–1180 nM), indicating that the substituted site on the quinoxaline backbone played a key role in the binding to Aβ aggregates. The most prospective [^{18}F]**127** showed intensive labeling of Aβ deposits in vivo in APP/PS1 mice, but associated with high non-specific binding in the white matter. The authors attributed this high non-specific radioactivity accumulation to the binding [^{18}F]**127** to the myelin sheaths in the white matter.

10. Conclusion

Based on the amyloid cascade hypothesis, searching for amyloid-avid imaging probes that can facilitate the early diagnosis of AD has been one of the major biomedical research efforts. A big

group of ThT derived benzoheterocyclic compounds have been synthesized and evaluated as Aβ imaging candidates. In this review, we provide a comprehensive view of these radioactive benzoheterocyclics for highlighting the Aβ plaques in the brain, covering the synthetic approaches to the benzoheterocyclic scaffold, binding potencies and brain pharmacokinetics of each ligand. These scaffolds were readily constructed through well-established synthetic strategies. Some of the benzoheterocyclic compounds presented encouraging in vivo imaging properties, and [^{11}C]PIB has emerged as the most promising one. To take the advantage of the longer half-life of fluorine-18, a wide variety of ^{18}F-labeled Aβ probes have been developed. Among them [^{18}F]GE-067 has been approved by U.S. FDA, and [^{18}F]AZD4694 and [^{18}F]MK-3328 are currently under late phases of clinical trials. Despite this progress, developing of a selective SPECT radiotracer to visualize Aβ plaques is pressingly needed. After the failure of [^{125}I]IMPY in clinical translation, the radioiodinated Aβ imaging agents have appeared no evolvement till now. On the other hand, progress with ^{99m}Tc-lebeled ligands is also quite limited for their poor BBB penetration.

Conflict of interest

The authors declare no conflict of interest.

Acknowledgment

This work was supported by National Natural Science Foundation of China (No: 21201019).

References

[1] C.L. Masters, R. Cappai, K.J. Barnham, V.L. Villemagne, Molecular mechanisms for Alzheimer's disease: implications for neuroimaging and therapeutics, J. Neurochem. 97 (2006) 1700–1725.
[2] D.J. Selkoe, Alzheimer's disease: genes, proteins, and therapy, Physiol. Rev. 81 (2001) 741–766.
[3] B.D. James, S.E. Leurgans, L.E. Hebert, P.A. Scherr, K. Yaffe, D.A. Bennett, Contribution of Alzheimer disease to mortality in the United States, Neurology 82 (2014) 1045–1050.
[4] M. Prince, M. Prina, M. Guerchet, World Alzheimer Report 2013: Journey of Caring — an Analysis of Long-term Care for Dementia, Sep 2013.
[5] J. Hardy, D.J. Selkoe, The amyloid hypothesis of Alzheimer's disease: progress and problems on the road to therapeutics, Science 297 (2002) 353–356.
[6] S.M. Ametamey, M. Honer, P.A. Schubiger, Molecular imaging with PET, Chem. Rev. 108 (2008) 1501–1516.
[7] M. Cui, Past and recent progress of molecular imaging probes for β-amyloid plaques in the brain, Curr. Med. Chem. 21 (2014) 82–112.
[8] M. Zhou, X. Wang, Z. Liu, L. Yu, S. Hu, L. Chen, W. Zeng, Advances of molecular imaging probes for the diagnosis of Alzheimer's disease, Curr. Alzheimer Res. 11 (2014) 221–231.
[9] T.J. Eckroat, A.S. Mayhoub, S. Garneau-Tsodikova, Amyloid-β probes: review of structure–activity and brain-kinetics relationships, Beilstein J. Org. Chem. 9 (2013) 1012–1044.
[10] C.A. Mathis, N.S. Mason, B.J. Lopresti, W.E. Klunk, Development of positron emission tomography β-amyloid plaque imaging agents, Semin. Nucl. Med. 42 (2012) 423–432.
[11] F. Zeng, M.M. Goodman, Fluorine-18 radiolabeled heterocycles as PET tracers for imaging beta-amyloid plaques in Alzheimer's disease, Curr. Top. Med. Chem. 13 (2013) 909–919.
[12] P.S. Vassar, C.F. Culling, Fluorescent stains, with special reference to amyloid and connective tissues, Arch. Pathol. 68 (1959) 487–498.
[13] M. Biancalana, S. Koide, Molecular mechanism of Thioflavin-T binding to amyloid fibrils, Biochim. Biophys. Acta 1804 (2010) 1405–1412.
[14] M. Biancalana, K. Makabe, A. Koide, S. Koide, Aromatic cross-strand ladders control the structure and stability of beta-rich peptide self-assembly mimics, J. Mol. Biol. 383 (2008) 205–213.
[15] C. Wu, Z. Wang, H. Lei, Y. Duan, M.T. Bowers, J.E. Shea, The binding of Thioflavin T and its neutral analog BTA-1 to protofibrils of the Alzheimer's disease Abeta (16–22) peptide probed by molecular dynamics simulations, J. Mol. Biol. 384 (2008) 718–729.
[16] C.A. Mathis, Y. Wang, D.P. Holt, G.-F. Huang, M.L. Debnath, W.E. Klunk, Synthesis and evaluation of ^{11}C-labeled 6-substituted 2-arylbenzothiazoles as amyloid imaging agents, J. Med. Chem. 46 (2003) 2740–2754.
[17] G. Henriksen, A.I. Hauser, A.D. Westwell, B.H. Yousefi, M. Schwaiger, A. Drzezga, H.-J. Wester, Metabolically stabilized benzothiazoles for imaging of amyloid plaques, J. Med. Chem. 50 (2007) 1087–1089.
[18] V. Facchinetti, R. da, R. Reis, C.R.B. Gomes, T.R.A. Vasconcelos, Chemistry and biological activities of 1,3-benzothiazoles, Mini Rev. Org. Chem. 9 (2012) 44–53.
[19] R. Leuma Yona, S. Mazères, P. Faller, E. Gras, Thioflavin derivatives as markers for amyloid-β fibrils: insights into structural features important for high-affinity binding, ChemMedChem 3 (2008) 63–66.
[20] J.X. Qiao, T.C. Wang, C. Hu, J. Li, R.R. Wexler, P.Y.S. Lam, Transformation of anionically activated trifluoromethyl groups to heterocycles under mild aqueous conditions, Org. Lett. 13 (2011) 1804–1807.
[21] S. Ranjit, X. Liu, Direct arylation of benzothiazoles and benzoxazoles with aryl boronic acids, Chem. Eur. J. 17 (2011) 1105–1108.
[22] D. Alagille, R.M. Baldwin, G.D. Tamagnan, One-step synthesis of 2-arylbenzothiazole ('BTA') and -benzoxazole precursors for in vivo imaging of β-amyloid plaques, Tetrahedron Lett. 46 (2005) 1349–1351.
[23] H. Bonin, R. Leuma-Yona, B. Marchiori, P. Demonchaux, E. Gras, Highly practical boronic acid surrogates for the Suzuki–Miyaura cross-coupling, Tetrahedron Lett. 52 (2011) 1132–1135.
[24] A.E. Johnson, F. Jeppsson, J. Sandell, D. Wensbo, J.A.M. Neelissen, A. Juréus, P. Ström, H. Norman, L. Farde, S.P.S. Svensson, AZD2184: a radioligand for sensitive detection of β-amyloid deposits, J. Neurochem. 108 (2009) 1177–1186.
[25] W.E. Klunk, Y. Wang, G.-f. Huang, M.L. Debnath, D.P. Holt, C.A. Mathis, Uncharged Thioflavin-T derivatives bind to amyloid-beta protein with high affinity and readily enter the brain, Life Sci. 69 (2001) 1471–1484.
[26] W.E. Klunk, H. Engler, A. Nordberg, Y. Wang, G. Blomqvist, D.P. Holt, M. Bergström, I. Savitcheva, G.-F. Huang, S. Estrada, B. Ausén, M.L. Debnath, J. Barletta, J.C. Price, J. Sandell, B.J. Lopresti, A. Wall, P. Koivisto, G. Antoni, C.A. Mathis, B. Långström, Imaging brain amyloid in Alzheimer's disease with Pittsburgh compound-B, Ann. Neurol. 55 (2004) 306–319.
[27] M.D. Ikonomovic, W.E. Klunk, E.E. Abrahamson, C.A. Mathis, J.C. Price, N.D. Tsopelas, B.J. Lopresti, S. Ziolko, W. Bi, W.R. Paljug, M.L. Debnath, C.E. Hope, B.A. Isanski, R.L. Hamilton, S.T. DeKosky, Post-mortem correlates of in vivo PiB-PET amyloid imaging in a typical case of Alzheimer's disease, Brain 131 (2008) 1630–1645.
[28] A. Kadir, A. Marutle, D. Gonzalez, M. Schöll, O. Almkvist, M. Mousavi, T. Mustafiz, T. Darreh-Shori, I. Nennesmo, A. Nordberg, Positron emission tomography imaging and clinical progression in relation to molecular pathology in the first Pittsburgh compound B positron emission tomography patient with Alzheimer's disease, Brain 134 (2011) 301–317.
[29] K. Serdons, T. Verduyckt, D. Vanderghinste, P. Borghgraef, J. Cleynhens, F. Van Leuven, H. Kung, G. Bormans, A. Verbruggen, ^{11}C-labelled PIB analogues as potential tracer agents for in vivo imaging of amyloid β in Alzheimer's disease, Eur. J. Med. Chem. 44 (2009) 1415–1426.
[30] S. Nyberg, M. Jönhagen, Z. Cselényi, C. Halldin, P. Julin, H. Olsson, Y. Freund-Levi, J. Andersson, K. Varnäs, S. Svensson, L. Farde, Detection of amyloid in Alzheimer's disease with positron emission tomography using [^{11}C]AZD2184, Eur. J. Nucl. Med. Mol. Imaging 36 (2009) 1859–1863.
[31] J.D. Andersson, K. Varnäs, Z. Cselényi, B. Gulyás, D. Wensbo, S.J. Finnema, B.-M. Swahn, S. Svensson, S. Nyberg, L. Farde, C. Halldin, Radiosynthesis of the candidate β-amyloid radioligand [^{11}C]AZD2184: positron emission tomography examination and metabolite analysis in cynomolgus monkeys, Synapse 64 (2010) 733–741.
[32] Z.P. Zhuang, M.P. Kung, C. Hou, D.M. Skovronsky, T.L. Gur, K. Plössl, J.Q. Trojanowski, V.M.Y. Lee, H.F. Kung, Radioiodinated styrylbenzenes and thioflavins as probes for amyloid aggregates, J. Med. Chem. 44 (2001) 1905–1914.
[33] U. Berndt, C. Stanetty, T. Wanek, C. Kuntner, J. Stanek, M. Berger, M. Bauer, G. Henriksen, H.-J. Wester, H. Kvaternik, P. Angelberger, C. Noe, Synthesis of a [^{18}F]fluorobenzothiazole as potential amyloid imaging agent, J. Label. Comp. Radiopharm. 51 (2008) 137–145.
[34] M.-Q. Zheng, D.-Z. Yin, J.-P. Qiao, L. Zhang, Y.-X. Wang, Syntheses and evaluation of fluorinated benzothiazole anilines as potential tracers for β-amyloid plaques in Alzheimer's disease, J. Fluor. Chem. 129 (2008) 210–216.
[35] M.-Q. Zheng, D.-Z. Yin, L. Zhang, B. Lei, D.-F. Cheng, H.-C. Cai, Y.-J. Han, M.-X. Wu, H. Zhang, J. Wang, Biological characters of [^{18}F]O-FEt-PIB in a rat model of Alzheimer's disease using micro-PET imaging, Acta Pharmacol. Sin. 29 (2008) 548–554.
[36] B. Neumaier, S. Deisenhofer, C. Sommer, C. Solbach, S.N. Reske, F. Mottaghy, Synthesis and evaluation of ^{18}F-fluoroethylated benzothiazole derivatives for in vivo imaging of amyloid plaques in Alzheimer's disease, Appl. Radiat. Isot. 68 (2010) 1066–1072.
[37] K. Serdons, D. Vanderghinste, M. Van Eeckhoudt, P. Borghgraef, H. Kung, F. Van Leuven, T. de Groot, G. Bormans, A. Verbruggen, Synthesis and evaluation of two fluorine-18 labelled phenylbenzothiazoles as potential in vivo tracers for amyloid plaque imaging, J. Label. Comp. Radiopharm. 52 (2009) 473–481.
[38] K.A. Stephenson, R. Chandra, Z.-P. Zhuang, C. Hou, S. Oya, M.-P. Kung, H.F. Kung, Fluoro-pegylated (FPEG) imaging agents targeting Aβ aggregates, Bioconjug. Chem. 18 (2006) 238–246.
[39] M. Cui, X. Wang, P. Yu, J. Zhang, Z. Li, X. Zhang, Y. Yang, M. Ono, H. Jia, H. Saji, B. Liu, Synthesis and evaluation of novel ^{18}F labeled 2-pyridinylbenzoxazole and 2-pyridinylbenzothiazole derivatives as ligands for positron emission

tomography (PET) imaging of β-amyloid plaques, J. Med. Chem. 55 (2012) 9283–9296.
[40] C. Mathis, B. Lopresti, N. Mason, J. Price, N. Flatt, W. Bi, S. Ziolko, S. DeKosky, W. Klunk, Comparison of the amyloid imaging agents [F-18]3′-F-PIB and [C-11]PIB in Alzheimer's disease and control subjects, J. Nucl. Med. 48 (Suppl. 2) (2007) 56.
[41] M. Koole, D.M. Lewis, C. Buckley, N. Nelissen, M. Vandenbulcke, D.J. Brooks, R. Vandenberghe, K. Van Laere, Whole-body biodistribution and radiation dosimetry of ^{18}F-GE067: a radioligand for in vivo brain amyloid imaging, J. Nucl. Med. 50 (2009) 818–822.
[42] A. Snellman, J. Rokka, F. Lopez-Picon, O. Eskola, I. Wilson, G. Farrar, M. Scheinin, O. Solin, J. Rinne, M. Haaparanta-Solin, Pharmacokinetics of [^{18}F] flutemetamol in wild-type rodents and its binding to beta amyloid deposits in a mouse model of Alzheimer's disease, Eur. J. Nucl. Med. Mol. Imaging 39 (2012) 1784–1795.
[43] S. Hatashita, H. Yamasaki, Y. Suzuki, K. Tanaka, D. Wakebe, H. Hayakawa, [^{18}F]Flutemetamol amyloid-beta PET imaging compared with [^{11}C]PIB across the spectrum of Alzheimer's disease, Eur. J. Nucl. Med. Mol. Imaging 41 (2014) 290–300.
[44] N. Nelissen, K. Van Laere, L. Thurfjell, R. Owenius, M. Vandenbulcke, M. Koole, G. Bormans, D.J. Brooks, R. Vandenberghe, Phase 1 study of the Pittsburgh compound B derivative ^{18}F-flutemetamol in healthy volunteers and patients with probable Alzheimer disease, J. Nucl. Med. 50 (2009) 1251–1259.
[45] R. Vandenberghe, K. Van Laere, A. Ivanoiu, E. Salmon, C. Bastin, E. Triau, S. Hasselbalch, I. Law, A. Andersen, A. Korner, L. Minthon, G. Garraux, N. Nelissen, G. Bormans, C. Buckley, R. Owenius, L. Thurfjell, G. Farrar, D.J. Brooks, ^{18}F-flutemetamol amyloid imaging in Alzheimer disease and mild cognitive impairment: a phase 2 trial, Ann. Neurol. 68 (2010) 319–329.
[46] K. Serdons, T. Verduyckt, D. Vanderghinste, J. Cleynhens, P. Borghgraef, P. Vermaelen, C. Terwinghe, F.V. Leuven, K.V. Laere, H. Kung, G. Bormans, A. Verbruggen, Synthesis of ^{18}F-labelled 2-(4′-fluorophenyl)-1,3-benzothiazole and evaluation as amyloid imaging agent in comparison with [^{11}C]PIB, Bioorg. Med. Chem. Lett. 19 (2009) 602–605.
[47] K. Serdons, C. Terwinghe, P. Vermaelen, K. Van Laere, H. Kung, L. Mortelmans, G. Bormans, A. Verbruggen, Synthesis and evaluation of ^{18}F-Labeled 2-phenylbenzothiazoles as positron emission tomography imaging agents for amyloid plaques in Alzheimer's disease, J. Med. Chem. 52 (2009) 1428–1437.
[48] K. Serdons, K. Van Laere, P. Janssen, H.F. Kung, G. Bormans, A. Verbruggen, Synthesis and evaluation of three ^{18}F-labeled aminophenylbenzothiazoles as amyloid imaging agents, J. Med. Chem. 52 (2009) 7090–7102.
[49] B.C. Lee, J.S. Kim, B.S. Kim, J.Y. Son, S.K. Hong, H.S. Park, B.S. Moon, J.H. Jung, J.M. Jeong, S.E. Kim, Aromatic radiofluorination and biological evaluation of 2-aryl-6-[^{18}F]fluorobenzothiazoles as a potential positron emission tomography imaging probe for β-amyloid plaques, Bioorg. Med. Chem. 19 (2011) 2980–2990.
[50] K. Serdons, T. Verduyckt, J. Cleynhens, C. Terwinghe, L. Mortelmans, G. Bormans, A. Verbruggen, Synthesis and evaluation of a ^{99m}Tc-BAT-phenylbenzothiazole conjugate as a potential in vivo tracer for visualization of amyloid β, Bioorg. Med. Chem. Lett. 17 (2007) 6086–6090.
[51] X. Chen, P. Yu, L. Zhang, B. Liu, Synthesis and biological evaluation of ^{99m}Tc, Re-monoamine-monoamide conjugated to 2-(4-aminophenyl)benzothiazole as potential probes for β-amyloid plaques in the brain, Bioorg. Med. Chem. Lett. 18 (2008) 1442–1445.
[52] K. Serdons, T. Verduyckt, J. Cleynhens, G. Bormans, A. Verbruggen, Development of ^{99m}Tc-Thioflavin-T derivatives for detection of systemic amyloidosis, J. Label. Comp. Radiopharm. 51 (2008) 357–367.
[53] K. Serdons, D. Vanderghinste, M. Van Eeckhoudt, J. Cleynhens, T. de Groot, G. Bormans, A. Verbruggen, Synthesis and evaluation of two uncharged ^{99m}Tc-labeled derivatives of Thioflavin-T as potential tracer agents for fibrillar brain amyloid, J. Label. Comp. Radiopharm. 52 (2009) 227–235.
[54] M. Sagnou, S. Tzanopoulou, C.P. Raptopoulou, V. Psycharis, H. Braband, R. Alberto, I.C. Pirmettis, M. Papadopoulos, M. Pelecanou, A phenylbenzothiazole conjugate with the tricarbonyl *fac*-[M(I)(CO)$_3$]$^+$ (M = Re, ^{99}Tc, ^{99m}Tc) core for imaging of β-amyloid plaques, Eur. J. Inorg. Chem. 2012 (2012) 4279–4286.
[55] C. Wu, J. Wei, K. Gao, Y. Wang, Dibenzothiazoles as novel amyloid-imaging agents, Bioorg. Med. Chem. 15 (2007) 2789–2796.
[56] M.-C. Cui, Z.-J. Li, R.-K. Tang, B.-L. Liu, Synthesis and evaluation of novel benzothiazole derivatives based on the bithiophene structure as potential radiotracers for β-amyloid plaques in Alzheimer's disease, Bioorg. Med. Chem. 18 (2010) 2777–2784.
[57] K. Matsumura, M. Ono, S. Hayashi, H. Kimura, Y. Okamoto, M. Ihara, R. Takahashi, H. Mori, H. Saji, Phenyldiazenyl benzothiazole derivatives as probes for in vivo imaging of neurofibrillary tangles in Alzheimer's disease brains, MedChemComm 2 (2011) 596–600.
[58] K. Matsumura, M. Ono, H. Kimura, M. Ueda, Y. Nakamoto, K. Togashi, Y. Okamoto, M. Ihara, R. Takahashi, H. Saji, ^{18}F-labeled phenyldiazenyl benzothiazole for in vivo imaging of neurofibrillary tangles in Alzheimer's disease brains, ACS Med. Chem. Lett. 3 (2011) 58–62.
[59] C. Gan, L. Zhou, Z. Zhao, H. Wang, Benzothiazole schiff-bases as potential imaging agents for β-amyloid plaques in Alzheimer's disease, Med. Chem. Res. 22 (2013) 4069–4074.
[60] Z.-P. Zhuang, M.-P. Kung, C. Hou, K. Plössl, D. Skovronsky, T.L. Gur, J.Q. Trojanowski, V.M.Y. Lee, H.F. Kung, IBOX(2-(4′-dimethylaminophenyl)-6-iodobenzoxazole): a ligand for imaging amyloid plaques in the brain, Nucl. Med. Biol. 28 (2001) 887–894.
[61] M. Terashima, M. Ishii, Y. Kanaoka, A facile synthesis of 2-substituted benzoxazoles, Synthesis 1982 (1982) 484–485.
[62] S.H. Hausner, D. Alagille, A.O. Koren, L. Amici, J.K. Staley, K.P. Cosgrove, R.M. Baldwin, G.D. Tamagnan, Synthesis of 5- and 6-substituted 2-(4-dimethylaminophenyl)-1,3-benzoxazoles and their in vitro and in vivo evaluation as imaging agents for amyloid plaque, Bioorg. Med. Chem. Lett. 19 (2009) 543–545.
[63] B.-M. Swahn, D. Wensbo, J. Sandell, D. Sohn, C. Slivo, D. Pyring, J. Malmström, E. Arzel, M. Vallin, M. Bergh, F. Jeppsson, A.E. Johnson, A. Juréus, J. Neelissen, S. Svensson, Synthesis and evaluation of 2-pyridylbenzothiazole, 2-pyridylbenzoxazole and 2-pyridylbenzofuran derivatives as ^{11}C-PET imaging agents for β-amyloid plaques, Bioorg. Med. Chem. Lett. 20 (2010) 1976–1980.
[64] B.-M. Swahn, J. Sandell, D. Pyring, M. Bergh, F. Jeppsson, A. Juréus, J. Neelissen, P. Johnström, M. Schou, S. Svensson, Synthesis and evaluation of pyridylbenzofuran, pyridylbenzothiazole and pyridylbenzoxazole derivatives as ^{18}F-PET imaging agents for β-amyloid plaques, Bioorg. Med. Chem. Lett. 22 (2012) 4332–4337.
[65] J. Chang, K. Zhao, S. Pan, Synthesis of 2-arylbenzoxazoles via DDQ promoted oxidative cyclization of phenolic Schiff bases—a solution-phase strategy for library synthesis, Tetrahedron Lett. 43 (2002) 951–954.
[66] M. Cui, M. Ono, H. Kimura, M. Ueda, Y. Nakamoto, K. Togashi, Y. Okamoto, M. Ihara, R. Takahashi, B. Liu, H. Saji, Novel ^{18}F-labeled benzoxazole derivatives as potential positron emission tomography probes for imaging of cerebral β-amyloid plaques in Alzheimer's disease, J. Med. Chem. 55 (2012) 9136–9145.
[67] N. Okamura, T. Suemoto, T. Shiomitsu, M. Suzuki, H. Shimadzu, H. Akatsu, T. Yamamoto, H. Arai, H. Sasaki, K. Yanai, M. Staufenbiel, Y. Kudo, T. Sawada, A novel imaging probe for in vivo detection of neuritic and diffuse amyloid plaques in the brain, J. Mol. Neurosci. 24 (2004) 247–255.
[68] N. Okamura, T. Suemoto, H. Shimadzu, M. Suzuki, T. Shiomitsu, H. Akatsu, T. Yamamoto, M. Staufenbiel, K. Yanai, H. Arai, H. Sasaki, Y. Kudo, T. Sawada, Styrylbenzoxazole derivatives for in vivo imaging of amyloid plaques in the brain, J. Neurosci. 24 (2004) 2535–2541.
[69] H. Shimadzu, T. Suemoto, M. Suzuki, T. Shiomitsu, N. Okamura, Y. Kudo, T. Sawada, Novel probes for imaging amyloid-β: F-18 and C-11 labeling of 2-(4-aminostyryl)benzoxazole derivatives, J. Label. Comp. Radiopharm. 47 (2004) 181–190.
[70] Y. Kudo, N. Okamura, S. Furumoto, M. Tashiro, K. Furukawa, M. Maruyama, M. Itoh, R. Iwata, K. Yanai, H. Arai, 2-(2-[2-Dimethylaminothiazol-5-yl] ethenyl)-6-(2-[fluoro]ethoxy)benzoxazole: a novel PET agent for in vivo detection of dense amyloid plaques in Alzheimer's disease patients, J. Nucl. Med. 48 (2007) 553–561.
[71] N. Okamura, S. Furumoto, Y. Funaki, T. Suemoto, M. Kato, Y. Ishikawa, S. Ito, H. Akatsu, T. Yamamoto, T. Sawada, H. Arai, Y. Kudo, K. Yanai, Binding and safety profile of novel benzoxazole derivative for in vivo imaging of amyloid deposits in Alzheimer's disease, Geriatr. Gerontol. Int. 7 (2007) 393–400.
[72] S. Furumoto, N. Okamura, K. Furukawa, M. Tashiro, Y. Ishikawa, K. Sugi, N. Tomita, M. Waragai, R. Harada, T. Tago, R. Iwata, K. Yanai, H. Arai, Y. Kudo, A ^{18}F-Labeled BF-227 derivative as a potential radioligand for imaging dense amyloid plaques by positron emission tomography, Mol. Imaging Biol. 15 (2013) 497–506.
[73] H. Ito, H. Shinotoh, H. Shimada, M. Miyoshi, K. Yanai, N. Okamura, H. Takano, H. Takahashi, R. Arakawa, F. Kodaka, M. Ono, Y. Eguchi, M. Higuchi, T. Fukumura, T. Suhara, Imaging of amyloid deposition in human brain using positron emission tomography and [^{18}F]FACT: comparison with [^{11}C]PIB, Eur. J. Nucl. Med. Mol. Imaging 41 (2014) 745–754.
[74] T. Kaneta, N. Okamura, A. Arai, K. Takanami, K. Furukawa, M. Tashiro, S. Furumoto, R. Iwata, S. Takahashi, H. Arai, K. Yanai, Y. Kudo, Analysis of early phase [^{11}C]BF-227 PET, and its application for anatomical standardization of late-phase images for 3D-SSP analysis, Jpn. J. Radiol. 32 (2014) 138–144.
[75] E.D. Hostetler, S. Sanabria-Bohórquez, H. Fan, Z. Zeng, L. Gammage, P. Miller, S. O'Malley, B. Connolly, J. Mulhearn, S.T. Harrison, S.E. Wolkenberg, J.C. Barrow, D.L. Williams Jr., R.J. Hargreaves, C. Sur, J.J. Cook, [^{18}F]Fluoroazabenzoxazoles as potential amyloid plaque PET tracers: synthesis and in vivo evaluation in rhesus monkey, Nucl. Med. Biol. 38 (2011) 1193–1203.
[76] S.T. Harrison, J. Mulhearn, S.E. Wolkenberg, P.J. Miller, S.S. O'Malley, Z. Zeng, D.L. Williams, E.D. Hostetler, S. Sanabria-Bohórquez, L. Gammage, H. Fan, C. Sur, J.C. Culberson, R.J. Hargreaves, J.J. Cook, G.D. Hartman, J.C. Barrow, Synthesis and evaluation of 5-fluoro-2-aryloxazolo[5,4-b]pyridines as β-amyloid PET ligands and identification of MK-3328, ACS Med. Chem. Lett. 2 (2011) 498–502.
[77] X. Wang, M. Cui, P. Yu, Z. Li, Y. Yang, H. Jia, B. Liu, Synthesis and biological evaluation of novel technetium-99m labeled phenylbenzoxazole derivatives as potential imaging probes for β-amyloid plaques in brain, Bioorg. Med. Chem. Lett. 22 (2012) 4327–4331.
[78] M. Ono, M.-P. Kung, C. Hou, H.F. Kung, Benzofuran derivatives as Aβ-aggregate-specific imaging agents for Alzheimer's disease, Nucl. Med. Biol. 29 (2002) 633–642.
[79] A. Hercouet, M. Le Corre, Une nouvelle voie d'accès aux benzofurannes, Tetrahedron Lett. 20 (1979) 2145–2148.

[80] M. Ono, Y. Cheng, H. Kimura, H. Watanabe, K. Matsumura, M. Yoshimura, S. Iikuni, Y. Okamoto, M. Ihara, R. Takahashi, H. Saji, Development of novel ^{123}I-labeled pyridyl benzofuran derivatives for SPECT imaging of β-amyloid plaques in Alzheimer's disease, PLoS One 8 (2013) e74104.

[81] M. Ono, H. Kawashima, A. Nonaka, T. Kawai, M. Haratake, H. Mori, M.-P. Kung, H.F. Kung, H. Saji, M. Nakayama, Novel benzofuran derivatives for PET imaging of β-amyloid plaques in Alzheimer's disease brains, J. Med. Chem. 49 (2006) 2725–2730.

[82] Y. Cheng, M. Ono, H. Kimura, S. Kagawa, R. Nishii, H. Kawashima, H. Saji, Fluorinated benzofuran derivatives for PET imaging of β-amyloid plaques in Alzheimer's disease brains, ACS Med. Chem. Lett. 1 (2010) 321–325.

[83] Y. Cheng, M. Ono, H. Kimura, S. Kagawa, R. Nishii, H. Saji, A novel ^{18}F-labeled pyridyl benzofuran derivative for imaging of β-amyloid plaques in Alzheimer's brains, Bioorg. Med. Chem. Lett. 20 (2010) 6141–6144.

[84] M. Ono, Y. Cheng, H. Kimura, M. Cui, S. Kagawa, R. Nishii, H. Saji, Novel ^{18}F-labeled benzofuran derivatives with improved properties for positron emission tomography (PET) imaging of β-amyloid plaques in Alzheimer's brains, J. Med. Chem. 54 (2011) 2971–2979.

[85] A. Juréus, B.-M. Swahn, J. Sandell, F. Jeppsson, A.E. Johnson, P. Johnström, J.A.M. Neelissen, D. Sunnemark, L. Farde, S.P.S. Svensson, Characterization of AZD4694, a novel fluorinated Aβ plaque neuroimaging PET radioligand, J. Neurochem. 114 (2010) 784–794.

[86] Z. Cselényi, M.E. Jönhagen, A. Forsberg, C. Halldin, P. Julin, M. Schou, P. Johnström, K. Varnäs, S. Svensson, L. Farde, Clinical validation of ^{18}F-AZD4694, an amyloid-β–specific PET radioligand, J. Nucl. Med. 53 (2012) 415–424.

[87] C.C. Rowe, S. Pejoska, R.S. Mulligan, G. Jones, J.G. Chan, S. Svensson, Z. Cselényi, C.L. Masters, V.L. Villemagne, Head-to-head comparison of ^{11}C-PiB and ^{18}F-AZD4694 (NAV4694) for β-amyloid imaging in aging and dementia, J. Nucl. Med. 54 (2013) 880–886.

[88] M. Schou, K. Varnäs, J. Sandell, P. Johnström, Z. Cselenyi, S. Svensson, R. Nakao, N. Amini, L. Bergman, A. Sumic, B. Gulyas, E. Lindström-Böö, C. Halldin, L. Farde, Synthesis, radiolabeling, and in vivo pharmacokinetic evaluation of the amyloid beta radioligand [^{11}C]AZD4694 in nonhuman primates, Mol. Imaging Biol. 16 (2014) 173–179.

[89] M. Ono, Y. Fuchi, T. Fuchigami, N. Kobashi, H. Kimura, M. Haratake, H. Saji, M. Nakayama, Novel benzofurans with ^{99m}Tc complexes as probes for imaging cerebral β-amyloid plaques, ACS Med. Chem. Lett. 1 (2010) 443–447.

[90] Y. Cheng, M. Ono, H. Kimura, M. Ueda, H. Saji, Technetium-99m labeled pyridyl benzofuran derivatives as single photon emission computed tomography imaging probes for β-amyloid plaques in Alzheimer's brains, J. Med. Chem. 55 (2012) 2279–2286.

[91] Y.S. Chang, J.M. Jeong, Y.-S. Lee, H.W. Kim, R.B. Ganesha, Y.J. Kim, D.S. Lee, J.-K. Chung, M.C. Lee, Synthesis and evaluation of benzothiophene derivatives as ligands for imaging β-amyloid plaques in Alzheimer's disease, Nucl. Med. Biol. 33 (2006) 811–820.

[92] H. Watanabe, M. Ono, M. Haratake, N. Kobashi, H. Saji, M. Nakayama, Synthesis and characterization of novel phenylindoles as potential probes for imaging of β-amyloid plaques in the brain, Bioorg. Med. Chem. 18 (2010) 4740–4746.

[93] N. Suzuki, S. Yasaki, A. Yasuhara, T. Sakamoto, Convenient indole synthesis from 2-iodoanilines and terminal alkynes by the sequential sonogashira reaction and the cyclization reaction promoted by tetrabutylammonium fluoride (TBAF), Chem. Pharm. Bull. 51 (2003) 1170–1173.

[94] H. Sano, T. Noguchi, A. Tanatani, Y. Hashimoto, H. Miyachi, Design and synthesis of subtype-selective cyclooxygenase (COX) inhibitors derived from thalidomide, Bioorg. Med. Chem. 13 (2005) 3079–3091.

[95] H. Fu, L. Yu, M. Cui, J. Zhang, X. Zhang, Z. Li, X. Wang, J. Jia, Y. Yang, P. Yu, H. Jia, B. Liu, Synthesis and biological evaluation of ^{18}F-labled 2-phenylindole derivatives as PET imaging probes for β-amyloid plaques, Bioorg. Med. Chem. 21 (2013) 3708–3714.

[96] B. Robinson, The Fischer indole synthesis, Chem. Rev. 63 (1963) 373–401.

[97] W. Qu, S.-R. Choi, C. Hou, Z. Zhuang, S. Oya, W. Zhang, M.-P. Kung, R. Manchandra, D.M. Skovronsky, H.F. Kung, Synthesis and evaluation of indolinyl- and indolylphenylacetylenes as PET imaging agents for β-amyloid plaques, Bioorg. Med. Chem. Lett. 18 (2008) 4823–4827.

[98] Y. Yang, H.-M. Jia, B.-L. Liu, (E)-5-styryl-1H-indole and (E)-6-styrylquinoline derivatives serve as probes for β-amyloid plaques, Molecules 17 (2012) 4252–4265.

[99] M.-P. Kung, C. Hou, Z.-P. Zhuang, B. Zhang, D. Skovronsky, J.Q. Trojanowski, V.M.Y. Lee, H.F. Kung, IMPY: an improved Thioflavin-T derivative for in vivo labeling of β-amyloid plaques, Brain Res. 956 (2002) 202–210.

[100] Z.-P. Zhuang, M.-P. Kung, A. Wilson, C.-W. Lee, K. Plössl, C. Hou, D.M. Holtzman, H.F. Kung, Structure–activity relationship of imidazo[1,2-*a*] pyridines as ligands for detecting β-amyloid plaques in the brain, J. Med. Chem. 46 (2002) 237–243.

[101] M.-P. Kung, C. Hou, Z.-P. Zhuang, D. Skovronsky, H.F. Kung, Binding of two potential imaging agents targeting amyloid plaques in postmortem brain tissues of patients with Alzheimer's disease, Brain Res. 1025 (2004) 98–105.

[102] K. Mei-Ping, H. Catherine, Z. Zhi-Ping, J.C. Alan, L.M. Donna, F.K. Hank, Characterization of IMPY as a potential imaging agent for β-amyloid plaques in double transgenic PSAPP mice, Eur. J. Nucl. Med. Mol. Imaging 31 (2004) 1136–1145.

[103] P.-J. Song, S. Bernard, P. Sarradin, J. Vergote, C. Barc, S. Chalon, M.-P. Kung, H.F. Kung, D. Guilloteau, IMPY, a potential β-amyloid imaging probe for detection of prion deposits in scrapie-infected mice, Nucl. Med. Biol. 35 (2008) 197–201.

[104] A.B. Newberg, N.A. Wintering, K. Plössl, J. Hochold, M.G. Stabin, M. Watson, D. Skovronsky, C.M. Clark, M.-P. Kung, H.F. Kung, Safety, biodistribution, and dosimetry of ^{123}I-IMPY: a novel amyloid plaque–imaging agent for the diagnosis of alzheimer's disease, J. Nucl. Med. 47 (2006) 748–754.

[105] B.H. Yousefi, A. Manook, B. von Reutern, M. Schwaiger, A. Drzezga, H.-J. Wester, G. Henriksen, Development of an improved radioiodinated 2-phenylimidazo[1,2-*a*]pyridine for non-invasive imaging of amyloid plaques, MedChemComm 3 (2012) 775–779.

[106] C.-J. Chen, K. Bando, H. Ashino, K. Taguchi, H. Shiraishi, O. Fujimoto, C. Kitamura, S. Matsushima, M. Fujinaga, M.-R. Zhang, H. Kasahara, T. Minamizawa, C. Jiang, M. Ono, M. Higuchi, T. Suhara, K. Yamada, B. Ji, Synthesis and biological evaluation of novel radioiodinated imidazopyridine derivatives for amyloid-β imaging in Alzheimer's disease, Bioorg. Med. Chem. 22 (2014) 4189–4197.

[107] L. Cai, F.T. Chin, V.W. Pike, H. Toyama, J.-S. Liow, S.S. Zoghbi, K. Modell, E. Briard, H.U. Shetty, K. Sinclair, S. Donohue, D. Tipre, M.-P. Kung, C. Dagostin, D.A. Widdowson, M. Green, W. Gao, M.M. Herman, M. Ichise, R.B. Innis, Synthesis and evaluation of two ^{18}F-labeled 6-iodo-2-(4′-N,N-dimethylamino)phenylimidazo[1,2-*a*]pyridine derivatives as prospective radioligands for β-amyloid in Alzheimer's disease, J. Med. Chem. 47 (2004) 2208–2218.

[108] F. Zeng, J.A. Southerland, R.J. Voll, J.R. Votaw, L. Williams, B.J. Ciliax, A.I. Levey, M.M. Goodman, Synthesis and evaluation of two ^{18}F-labeled imidazo[1,2-*a*] pyridine analogues as potential agents for imaging β-amyloid in Alzheimer's disease, Bioorg. Med. Chem. Lett. 16 (2006) 3015–3018.

[109] N. Seneca, L. Cai, J.-S. Liow, S.S. Zoghbi, R.L. Gladding, J. Hong, V.W. Pike, R.B. Innis, Brain and whole-body imaging in nonhuman primates with [^{11}C] MeS-IMPY, a candidate radioligand for β-amyloid plaques, Nucl. Med. Biol. 34 (2007) 681–689.

[110] F. Zeng, D. Alagille, G.D. Tamagnan, B.J. Ciliax, A.I. Levey, M.M. Goodman, Synthesis and in vitro evaluation of imidazo[1,2-*b*]pyridazines as ligands for β-Amyloid plaques, ACS Med. Chem. Lett. 1 (2010) 80–84.

[111] D. Alagille, H. DaCosta, R.M. Baldwin, G.D. Tamagnan, 2-Arylimidazo[2,1-*b*] benzothiazoles: a new family of amyloid binding agents with potential for PET and SPECT imaging of Alzheimer's brain, Bioorg. Med. Chem. Lett. 21 (2011) 2966–2968.

[112] B.H. Yousefi, A. Manook, A. Drzezga, B.von. Reutern, M. Schwaiger, H.J. Wester, G. Henriksen, Synthesis and evaluation of ^{11}C-labeled imidazo [2,1-*b*]benzothiazoles (IBTs) as PET tracers for imaging β-amyloid plaques in Alzheimer's disease, J. Med. Chem. 54 (2011) 949–956.

[113] B.H. Yousefi, A. Drzezga, B.von. Reutern, A. Manook, M. Schwaiger, H.J. Wester, G. Henriksen, A novel ^{18}F-labeled imidazo[2,1-*b*]benzothiazole (IBT) for high-contrast PET imaging of β-amyloid plaques, ACS Med. Chem. Lett. 2 (2011) 673–677.

[114] M. Cui, M. Ono, H. Kimura, H. Kawashima, B.L. Liu, H. Saji, Radioiodinated benzimidazole derivatives as single photon emission computed tomography probes for imaging of β-amyloid plaques in Alzheimer's disease, Nucl. Med. Biol. 38 (2011) 313–320.

[115] N. Vasdev, P. Cao, E.M. van Oosten, A.A. Wilson, S. Houle, G. Hao, X. Sun, N. Slavine, M. Alhasan, P.P. Antich, F.J. Bonte, P. Kulkarni, Synthesis and PET imaging studies of [^{18}F]2-fluoroquinolin-8-ol ([^{18}F]CABS13) in transgenic mouse models of Alzheimer's disease, MedChemComm 3 (2012) 1228–1230.

[116] N. Okamura, T. Suemoto, S. Furumoto, M. Suzuki, H. Shimadzu, H. Akatsu, T. Yamamoto, H. Fujiwara, M. Nemoto, M. Maruyama, H. Arai, K. Yanai, T. Sawada, Y. Kudo, Quinoline and benzimidazole derivatives: candidate probes for in vivo imaging of tau pathology in Alzheimer's disease, J. Neurosci. 25 (2005) 10857–10862.

[117] T. Tago, S. Furumoto, N. Okamura, R. Harada, Y. Ishikawa, H. Arai, K. Yanai, R. Iwata, Y. Kudo, Synthesis and preliminary evaluation of 2-arylhydroxyquinoline derivatives for tau imaging, J. Label. Comp. Radiopharm. 57 (2014) 18–24.

[118] M.T. Fodero-Tavoletti, N. Okamura, S. Furumoto, R.S. Mulligan, A.R. Connor, C.A. McLean, D. Cao, A. Rigopoulos, G.A. Cartwright, G. O'Keefe, S. Gong, P.A. Adlard, K.J. Barnham, C.C. Rowe, C.L. Masters, Y. Kudo, R. Cappai, K. Yanai, V.L. Villemagne, ^{18}F-THK523: a novel in vivo tau imaging ligand for Alzheimer's disease, Brain 134 (2011) 1089–1100.

[119] N. Okamura, S. Furumoto, R. Harada, T. Tago, T. Yoshikawa, M. Fodero-Tavoletti, R.S. Mulligan, V.L. Villemagne, H. Akatsu, T. Yamamoto, H. Arai, R. Iwata, K. Yanai, Y. Kudo, Novel ^{18}F-labeled arylquinoline derivatives for noninvasive imaging of tau pathology in Alzheimer disease, J. Nucl. Med. 54 (2013) 1420–1427.

[120] M. Cui, M. Ono, H. Kimura, B. Liu, H. Saji, Novel quinoxaline derivatives for in vivo imaging of β-amyloid plaques in the brain, Bioorg. Med. Chem. Lett. 21 (2011) 4193–4196.

[121] P. Yu, M. Cui, X. Wang, X. Zhang, Z. Li, Y. Yang, J. Jia, J. Zhang, M. Ono, H. Saji, H. Jia, B. Liu, ^{18}F-Labeled 2-phenylquinoxaline derivatives as potential positron emission tomography probes for in vivo imaging of β-amyloid plaques, Eur. J. Med. Chem. 57 (2012) 51–58.

[122] M. Yoshimura, M. Ono, K. Matsumura, H. Watanabe, H. Kimura, M. Cui, Y. Nakamoto, K. Togashi, Y. Okamoto, M. Ihara, R. Takahashi, H. Saji, Structure–activity relationships and in vivo evaluation of quinoxaline derivatives for PET Imaging of β-amyloid plaques, ACS Med. Chem. Lett. 4 (2013) 596–600.